2008

Stress analysis of wood-framed low-rise buildings under wind loads due to tornados

Nikhil Kumar
Iowa State University

Stress analysis of wood-framed low-rise buildings under wind loads due to tornados

by

Nikhil Kumar

A thesis submitted to the graduate faculty

in partial fulfillment of the requirements for the degree of

MASTER OF SCIENCE

Major: Aerospace Engineering

Program of Study Committee:
Vinay Dayal, Major Professor
Partha Sarkar
William Gallus

Iowa State University

Ames, Iowa

2008

TABLE OF CONTENTS

LIST OF FIGURES

LIST OF TABLES

ABSTRACT

Buildings in the "tornado alley" of the United States, an area where tornados occur most frequently, are built to withstand 3-sec wind speeds of 90 mph, whereas 90% of the tornados reported generate anywhere from 40 to 157 mph. At the same time, these codes are based mostly on studying the effects of straight line winds and not on tornado type winds on buildings, especially on low-rise, wood framed buildings which make up the majority of structures in the United States. Previous research at Iowa State University (ISU) includes extensive testing on a scaled down low-rise gable roof building model (1:100) to understand tornado induced loading pattern as the tornado sweeps past the building. This study was performed using the ISU tornado simulator for various building models and orientations subjected to different tornado speeds and vortex cores. In this work Finite Element models were developed using ANSYS for full-scale numerical gable roof buildings with three different roof angles (13.4^0, 25.5^0 and 35.1^0). The tornado-induced wind loads recorded in the laboratory experiments were applied to the models to determine the detailed stress distribution over them. This numerical study was performed using the same parameter as in the laboratory experiments such as those listed earlier. In the next phase of this research work a routine was developed in ANSYS to incorporate a failure criterion for the building models to assess its damage potential and resulting debris formation. Composite movie sets were created showing the stress distribution over the buildings as the tornado goes past it and also the pattern of debris generation and the order in which the building gets damaged.

CHAPTER 1. INTRODUCTION

Tornados are violently rotating columns of air extending from a thunderstorm to the ground. Though they occur in many parts of the world, they are found to occur most frequently in the United States. There are around a thousand tornados reported annually in the U.S, causing around 60 fatalities each year and thousands of injuries (Grazulis 1993). They cause damage of more than a billion dollars every year. Though tornados have occurred in all fifty states, they are concentrated in what is known as the "tornado alley", located in the central region. According to the current design codes, low-rise buildings are built to withstand only up to 90 mph of straight-line winds, when 90% of the tornados reported generate anywhere from 40 to 157 mph. At the same time, these codes are based on studying the effects of straight line winds and not on tornado type winds on buildings, especially on low-rise, wood framed buildings which make up the majority of structures in the U.S. Also, the property damages that occur due to tornados are significant due to wind-borne debris similar to the direct effect of high speed wind on them. It is therefore necessary to assess the wind damage potential of buildings as a function of distribution of local wind speed and map the generation of wind-borne debris from the buildings. Previous research was to carry out extensive wind tunnel tests on these types of structures under tornado type winds to obtain the forces acting on them. These tests were done on low-rise building models with a variety of commonly used roof angles and shapes. The main objective of this research work was to apply these tornado-induced wind loads, obtained in the laboratory using a scaled model of a low-rise building, to a numerical finite element model (FEM) of the building to assess its damage potential and resulting debris formation. The loads are applied in the quasi-static

manner, i.e. the experimental loads at discrete steps are applied to the building and analysis performed to calculate the loads and failure criteria is applied to ascertain the integrity of the elements. This work is limited due to the fact that the experimental work did not include the failure of the building due to tornadic loads and hence the pressure distribution has always been for an intact building while in this work the loads are applied to the damaged building as if the building was undamaged.

CHAPTER 2. PREVIOUS WORK

A lot of work has been done to deal with 3-D performances of timber frame buildings. One of the first analytical models were developed by Tuomi and McCutheon(1978) which assumes linear elastic behavior of nails. The nail deformation here is defined by the relative deformation of sheathing and frame at each point. Gupta and Kuo (1987) presented a linear building model with shear wall elements using nine degrees of freedom and seven superelements. This model used a strain energy formulation and analyzed the building tested by Tuomi and McCutheon. Foschi (1977) developed a finite element model which included nonlinear load-deflection properties for fastners. Frame elements were modeled linear and sheathing elements were modeled elastic and orthotropic. Kasal (1992) used the finite element software ANSYS to develop a three dimensional model. It consists of linear orthotropic 2-D shell elements and fasteners represented by three 1-D spring elements at each node. The properties of nails when pulled out and pulled through plywood and OSB boards were studied by Hergoz. He et al (2001) developed a 3D model using the FE technique with plate, beam, and nonlinear nail connections.

Extensive experimental work has already been carried out by other researchers using tornado simulator at the Wind Simulation and Testing Laboratory (WIST) at Iowa State University. The tornado simulator consists of a circular duct, 5.49m (18 ft.) in diameter and 3.35m (11 ft.) high, that is suspended from a 4500 kg (5 ton) overhead crane so that it can translate along a 10.36m (34 ft.) long ground plane. A 1.83m diameter fan (maximum flow rate of the fan is 40.0 m^3/s, 85,000 cfm) is mounted at the center of an inside duct to produce an updraft. A rotating downdraft is generated by redirecting the air from the updraft fan down through a 0.30m (1.0 ft.) wide annular duct of 5.49 m (18 ft) outside diameter. Rotation is

imparted to the air in the duct with vanes at the top of the simulator. As the rotating air flows toward the center of the simulator, the fan updraft stretches the low-level vorticity into a tornado-like vortex. The maximum translation speed of the crane is 0.61 m/s (2 ft/sec). Accounting for the acceleration and deceleration distance at the beginning and end of the crane motion, the prototype simulator can translate for a distance of 3.35 m (11 ft) at a constant speed of 0.61 m/s (1.4 mph) or less. More details on the design and validation of this tornado simulator can be found in Haan et al. (2007). As reported in Table 1, the building was subjected to moving tornado of five different swirl ratios (S). The ground plane was fixed at 45.7 cm (18 in.) below the exit of the downdraft duct and the fan speed was fixed at 33% of full speed. Data were sampled at the rate of 78 Hz for 26 seconds (due to data rate and storage limitations). Measurements were made for four vane angle settings. Maximum tangential velocities varied from 6.9 m/s to 9.7 m/s. The various tornado parameters like vortex radii, swirl ratios and flow rates and model Reynolds numbers are listed in Table 1. Vortex-induced pressures were measured on a model one-story gable roof building (nominally 1:100 scale) with a 91mm by 91mm (3.6 in. by 3.6 in.) plan and an eave height of 36mm (1.4 in). The model was constructed with Plexiglas surface and contains pressure taps to measure the overall external pressure distribution. Figures 1 sand 2 show the building pressure model with the pressure tap distribution. The roof contains a total of 54 pressure taps. The leeward side of the roof when the building is fixed at zero orientation with respect to the translational direction of the vortex, contains 24 pressure taps. The windward side contains 19 pressure taps and the two triangular gable end sections contain 5 taps each and the building walls contain 9 pressure taps on each side. The surface pressures were measured using a high speed electronic pressure scanner. Tests were done on the pressure model to

study the effects of different building orientations and the effects of various tornado sizes and translation velocities. The pressure model was tested with five different vortex sizes and in orientations with respect to the tornado translation axis from 0 to 90 degrees with a step size of 15 degrees. Figure 3 shows the building orientation with respect to the tornado translation axis. In each case tested, the tornado translation axis passed through the center of the building model. For all building orientations, four different cases of tornado translation speeds 0.15, 0.30, 0.46 and 0.61 m/sec (the fastest speed possible with the current system) were used. Each test conditions involved 10 repeat runs to study the statistical variance. In total, 140 different combinations of conditions were tested for each building model. Of the five 1-story building models tested, three of them are taken into discussion for further research, namely the one-story gable roof with 13.4^0, 25.5^0 and 35.1^0 roof angles. The resulting pressure distribution was then converted to full-scale values. The conversion values are shown in Table 2. More details on conversion to full-scale values can be found in Haan et al. (2007).

CHAPTER 3. MODELING THE BUILDING

The numerical model was designed so as to reflect the behavior of a typical American residential type, wood frame and low-rise gable roofed building as close as possible. The FEA package ANSYS was used to develop a mathematical model of the building. Different types of elements were used to represent the various parts of the building such as the 2x4s, nails and plywood cladding. There were 5 different types of elements that were used in the model. (1) 3-D beam element to simulate the 2x4s, (2) 3-D layered shell for the walls and roof split into layers for drywall, insulation and the outer plywood. The plywood can also be substituted for Oriented Standard Boards (OSB) by just changing the properties (Young's modulus and Poisson's ratio) in the layered shell element. (3), (4) and (5) three spring-damping elements, for a nail to take effect in each of the UX, UY and UZ direction.

3.1 ELEMENT TYPES USED

3.1.1 FRAME

The framework of 2X4s is represented by using the BEAM4 element available in ANSYS. BEAM4 is a 3D element with tension, compression, torsion, and bending capabilities as shown in Figure 4. The element is capable of six degrees of freedom at each node: translations in the nodal x, y, and z directions and rotations about the nodal x, y, and z axes. Each BEAM4 element is defined by three nodes (I, J and K), the cross-sectional area, two area moments of inertia (IZZ and IYY), two thicknesses (TKY and TKZ), an angle of orientation (θ) about the element x-axis, the torsional moment of inertia (IXX), and the

material properties. The element x-axis is oriented from node I toward node J. The node K defines a plane (with I and J) containing the element x and z axes. If K is not defined, θ=0° and orientation of the element y-axis is automatically calculated to be parallel to the global X-Y plane.

3.1.2 PLYWOOD SHEATHING

The sheathing was represented by using the SHELL93 element type, which is defined as an 8-node structural shell. This element is capable of six degrees of freedom at each node: translations in the nodal x, y, and z directions and rotations about the nodal x, y, and z axes. The deformation shapes are quadratic in both in-plane directions. The element has plasticity, stress stiffening, large deflection, and large strain capabilities.

3.1.3 NAILS

The element type used to represent the nails was the COMBIN39 element type. COMBIN39 is a unidirectional element with nonlinear generalized force-deflection capability that can be used in any analysis. The element has longitudinal or torsional capability in one, two, or three dimensional applications. The longitudinal option is a uniaxial tension-compression element with up to three degrees of freedom at each node: translations in the nodal x, y, and z directions. No bending or torsion is considered. The torsional option is a purely rotational element with three degrees of freedom at each node: rotations about the nodal x, y, and z axes. This element has no mass capabilities. This element was defined by

two node points and a generalized force-deflection curve. The points on this curve (D1, F1, etc.) represent force versus relative translation for structural analyses.

3.2 NAIL PULL-OUT TEST

In a timber structure like the one that was developed, all components like the roof panels, 2 x 4's and plywood claddings are held together with nails. A realistic numerical model required the knowledge of the load-displacement response of the nails. The nail response was first studied using the nail-pull test that was conducted using the Universal Testing Machine. Two pieces of 2 by 4's were nailed to each other and were pulled apart and the axial load vs. axial stroke measured. This setup is shown in Figure 5. These tests were performed many times and average response value has been determined for use in the model. It is needs to be noted that these tests were performed for one nail type and one wood type. If any one of the two parameters is changed, the response will be different. Results show that as the nail is pulled, it sustains the entire load initially. When the load increases such that it is larger than the friction between the wood and nail, the nail starts to pull out of the wood. During this stage, as the nail comes out of the wood, the embedded length reduces and as a result the friction reduces and it is progressively easier for the nail to be pulled out of the wood. This shows up as a reduction in the pull load in Figure 6. Thus, the nail pullout displays a non-linear load displacement behavior.

3.3 MODEL DESCRIPTION

The three mentioned element types, BEAM4, SHELL93 and COMBIN39 were used to model the building. The frame of 2x4s was modeled using the Density, Elastic modulus, Poisson's ratio of Douglas-fir lumber. For the present analysis, the beam was assumed to be isotropic in nature. The self-weight of the frame work was also applied. The cross-section of 2x4s is supposed to be 2" by 4", the processed lumber measures only 1.5" by 3.5" and hence these dimensions are used in the analysis. The area (A) and second moment of Inertias (IZZ and IYY) were calculated to be 5.25 sq.in, 5.3594 in^4 and 0.98435 in^4. The building has a square plan form of 75ft by 75ft with the 2X4s placed vertically at every 16". The K nodes (as mentioned in the "BEAM4" definition) of the 2X4s are defined such that the narrow faces of the 2X4 are oriented outward. The height of a single story is 9ft after which the roof starts. The vertical 2X4s are enclosed by a set of sole plates and top plates as shown in Figure 7. The roof was modeled using a "gable" truss as shown in Figures 8 and 9. This can also be modified if required for other types of trusses commonly used such as "W", "M", and "Scissors" etc. The distance between each truss structure of the roof was kept at 32" as can be seen from Figures 9 and 10. The Isometric view of the completed 2X4 framework is shown in Figure 11. The framework is covered by plywood sheathing before meshing. The sheathing was drawn on as areas around the frame as shown in Figure 12 and then meshed later. SHELL93 was used to model the plywood as defined earlier. The total mass of the plywood sheathing was included as mass per unit area and the thickness was kept at 0.5 in. The material properties used were that of Douglas-Fir plywood and was assumed to be Isotropic for this analysis.

One of the main requirements of meshing is to have the appropriate mesh type and mesh density. The mesh influences the accuracy, convergence and speed of the solution. This was mainly decided on the basis of the nail and 2X4 spacing. Another main requirement is that after meshing, the nodes of the 2X4 frame and plywood sheathing should coincide so that the nail element could be installed between them. The resulting building model after meshing is shown in Figures 13 and 14. This meshed model now has the nodes of the external plywood and 2X4s coinciding at around 16" intervals. Three nail elements are installed at every coincident node one to act in each of the UX, UY and UZ directions. Since the nail (COMBIN39) element type does not have mass capabilities, the mass of the nails were distributed among the mass of the plywood sheathing. This information was obtained from the experimental nail-pull analysis conducted earlier. All the nodes at Y=0 are constrained in all directions to serve as the base. This means that the foundation was not simulated as flexible but fully constrained. This may result in the stress changing in and around the foundation elements but the results of the upper part of the building will be unaffected. Three gable building models were designed to be tested as shown in Table 3.

3.4 CONVENTIONS USED TO PRESENT DATA

Since this analysis is about the numerical modeling of a previous experiment, the same conventions are used in representing the distance between tornados and the building models. Many of the figures in this thesis reflect the time-varying character of the tornado-induced loads. Rather than plotting these load histories with respect to time, these are plotted with respect to the distance between the center of the tornado vortex and the center of the

building model (x) normalized by the diameter of the tornado core (D). In all cases, the tornado translates along the x-axis in the positive x direction starting from x/D values less than -6.

3.5 CONVERTING PRESSURE DATA

The scaled down model used in experiment was constructed with plexiglass surface and contains pressure taps to measure the overall external pressure distribution. . Figures 1 and 2 show the building pressure model with the pressure tap distribution. The roof contains a total of 54 pressure taps. The leeward side of the roof (when the building is fixed at zero orientation with respect to the translational direction of the vortex, Figure 3) contains 24 pressure taps. The windward side contains 19 pressure taps and the two triangular gable end sections contain 5 taps each and the building walls contain 9 pressure taps on each side. It was assumed that the area immediately surrounding each pressure tap had the same value of pressure. There were 89 pressure taps on the experimental model, and hence the building model is taken to have 89 regions on its surfaces. The ANSYS code selects the nodes surrounding the location of the corresponding pressure tap, selects the elements associated with those nodes and then groups those elements under the corresponding pressure tap's number as shown in Figure 15.

The pressure data obtained from the experiment now has to be converted to ANSYS readable format. From the results of the experimental procedure, it was observed that the tornado does not have any effect on the pressure distribution when it is in the range of the first 30% of data as shown in an example in Figure 16 (circled) shows time histories of *Cp* on

the walls of the building model (Wall ports # 5, 14, 23 and 32) for Case 1 (0° building orientation with the smallest vortex size (Vane 1/ 15^0 vane angle) and slowest vortex translation speed (0.15 m/s)). The flat portion of the signal (for large negative values of x/D) corresponds to the situation where the tornado simulator's downdraft duct has not yet reached the model. This part of the data was not used as it only takes up more analysis time in ANSYS but does not affect the results.

A sub-routine was written using MATLAB to prepare the raw data files from the experiment into ANSYS readable format. Each test condition in the experiment involved 10 repeat runs to study the statistical variance. Each of those 10 result files has anywhere from 5000 to 20,000 values for each pressure port measured as the tornado moves over the building. The number of values depend on the crane speed (slower crane speeds generate lesser data as the data acquisition rate remains the same always). Solving the finite element model for each of these thousands of steps would require high computational power and time for every single run and not feasible. Hence, it was decided to solve a load step for every 0.5 second and so the data set was divided into 72 "Load Steps" as the tornado traverses over the building model. Each load step selects the individual region around the specific pressure tap location and assigns the respective pressure data to it. The MATLAB routine also converts the values from the experiment to full-scale values using the conversion values as derived by Haan et al before assigning the data to the specific regions. As mentioned, these conversion values are shown in Table 2.

CHAPTER 4. TEST PROCEDURE

Two major types of tests were conducted on the building models. The first test was done without any failure condition imposed on the building and the second with a sub-routine having specific failure criteria for every part of the building. Three different model buildings were tested namely the one-story gable roof with 13.4^0, 25.5^0, 35.1^0 roof angles as shown in Figures 17, 18 and 19. The experimental analysis was first done on the 35.1^0 gable roof for all vane angles. The results from that case clearly showed higher loads occurring for Vane 1, which corresponds to the tornado with smaller core radius. So the experiments for all the other different building models were tested with smaller core radius (Vane 1). This was followed for the numerical analysis too. The 35.1^0 model was tested with three vane angles (vane angle 15^0, 35^0, 55^0) and the 13.4^0 gable and 25.5^0 gable roof building were tested with the smallest vane angle available (vane 1, 15^0 vane angle). Each of the three building models at each orientation and vane angle were tested twice, one with slower moving tornado and with a faster moving tornado. The translational speeds (TS) of these tornados are the converted values from the experimental analysis using the conversion values provided. Since the time scale between the model and full-scale building is one and that the time scale can be defined as the length scale over velocity scale, they both have the same value. The model is 1:100 scale and hence the tornado translational velocity used for the experimental work is multiplied by value of 100 for converting it to full-scale. Refer to Haan et al. for more details on converting to full-scale values. The converted tornado translational speed (TS) values are shown in Table 4. All three building models were tested under both the conditions (with/-without failure criteria).

4.1 ANALYSIS WITHOUT FAILURE CRITERIA

This analysis was mainly performed to get the stress distribution over the building model. Using a MATLAB sub-routine, the selected data sets were loaded onto ANSYS as "Load Step" files which could be accessed collectively at any time step of the dynamic analysis. The ANSYS routine selects the building, assigns the first load step and solves it. The solver is then restarted from the end of the first load step and the program now solves for the second load step as a continuation. Each load was applied initially in 5 sub-steps and made to stop if the solution did not converge after 1000 sub-steps. The test matrix is shown in Table 5. These sequential stress distribution images can be made into a composite movie to understand the stress patterns the buildings undergo as the tornados pass over them for the different orientations, swirl ratios (vane angle) and translational speeds.

4.2 ANALYSIS WITH FAILURE CRITERIA

Separate code was written in ANSYS for solving this problem. The selected data sets were loaded onto ANSYS as "Load Step" files which could be accessed collectively at any time step of the dynamic analysis. The sub-routine would first solve for the first load step and then check each of the 3 element types one by one for failure. It would first select the shell elements (representing the plywood cladding) and check if the von-misses stresses in these elements are within the allowable limit. Similarly, it checks if any of the 2x4 beams (*beam4* elements) have buckled and then if any of the nail elements (*combin39* elements) have failed or have been pulled out (by using the results of the nail pull-out experiment as the criterion). All the elements that have failed are then saved into a database. The solver is then

restarted from the end of the first load step and those elements that have failed are deactivated, which makes them inactive during the second load step. This step of selecting the failed elements at the end of a load step and deactivating them was done by using the "ekill" command in ANSYS. A deactivated element remains in the model but contributes a near-zero stiffness value to the overall matrix. Deactivated elements contribute nothing to the overall mass matrix. The program now solves for the second load step. This procedure is now repeated for subsequent load steps, recording at each level the elements that have failed and deactivating them before starting the next step. A composite movie can now be generated which shows the sequential damage as the tornado goes past the building. The elements that fail and the order in which they fail as the tornado goes past will give us an insight to the type of wind-borne debris generated and their locations on the structure. The pressure recorded in the wind tunnel that is being used as the input here was for a fully intact model. Now since the structural stiffness changes as the elements fail, it will not be correct to use the same pressure data for the damaged structure. This analysis thus has this approximation built in. Hence, the solver was stopped after around 10 to 12 load steps for each case. Also each load was applied initially in 5 sub-steps and made to stop if the solution does not converge after 1000 sub-steps. The test matrix is shown in Table 6.

CHAPTER 5. RESULTS AND DISCUSSION

Initially, the tests were run without indicating any failure criteria for any of the three element types – The 2X4s, the nail elements or the plywood shell surrounding the framework. This was done to find any changes in the stress distribution pattern on the buildings. The peak stress encountered on all thirty cases is plotted in Figure 20. It is observed that all the buildings that experience tornado forces with smaller vane angles (Vane 1) have higher peak stresses than those that experience tornado forces with higher vane angles (Vane 3(35^0)) and Vane 5(55^0)). While comparing between the three buildings (13.4^0 gable, 25.5^0 gable and 35.1^0 gable) tested under same vane angle (Vane 1/ Vane 15^0), the peak stresses encountered by the 25.5^0 gable roof in all cases is the maximum. Also, the peak stresses for the 13.4^0 gable roof building is more than what was undergone by the 35.1^0 gable roof in all cases except for the 90^0 orientation with a 15.0 m/sec tornado translational speed.

A graph of the location of the tornado with respect to the center of the building when the maximum stress occurs is plotted in Figure 21. This clearly shows that in almost all the cases, the peak stress on the building is felt only after the center of the tornado crosses the center of the building i.e. *x/D* is greater than zero. Although *x*/D is around 0.3 on an average for slower moving tornados, this phenomenon is felt even more for faster moving ones. Here the average *x*/D value where the building undergoes maximum stress is around 1.4. A possible cause for the peak stress to occur after the center of the tornado has cleared the center of the building is given in Haan et al. that a fast moving tornado has the lower portion of the vortex lagging behind the upper portion. The faster moving vortex exhibits a greater *x*-direction shift compared to the slower moving vortex. A set of 30 composite movies were created (one for each case) showing the stress distribution pattern as the tornado moves past

the building. A screenshot taken when the building is under peak stress is shown for all the cases from Figure 22 to Figure 26. From this we can infer that the maximum stresses occur on the sides, at the junctions where the roof meets the walls (eaves) and at the top (ridge), where the two halves of the roofs meet. There is also high stress concentration about half way between the roof edge and the roof center which is at $1/4^{th}$ the total length of the roof. When comparing between 13.4^0, 25.5^0 and 35.1^0, there is lesser stress on the ridge of the roof for higher roof angles. Another noticeable difference is that the stresses halfway between the eaves and the ridge decrease with the increase in roof angle. Also, as the roof angle increases, the gable area increases and the stresses there become more prominent.

After this analysis, the buildings were tested with the failure criteria as described before. The ANSYS routine records the number of elements deleted as the tornado moves past the building for each load step. It should be emphasized that an element is a mathematical entity and hence its failure does not mean that the entire entity has failed. So if an element of the roof panel fails, the panel may not have completely failed. On the other hand when the nail element fails we can safely conclude that the nail has pullout is complete and denotes a complete failure. The total number of elements deleted vs. *x*/D for the five cases (13.4^0 gable roof with 15^0 Vane angle, 25.5^0 gable roof with 15^0 Vane angle, 35.1^0 gable roof with 15^0 Vane angle, 35.1^0 gable roof with 35^0 Vane angle, and 13.4^0 gable roof with 55^0 Vane angle) are plotted in Figures 27 to Figure 31. There are anywhere from 14,000 to 32,000 elements in total in the whole building depending on the building type (13.4^0, 25.5^0 or 35.1^0 gable). This includes all the three element types (2X4, nail and Shell). From the graphs, the maximum number of elements deleted is around 6000 and an average of 3000 for every run. This is a considerable amount of damage and makes up of about 10% of the total

building and it will not be correct to continue using the same pressure data for the damaged structure. Comparing the Figures 27, 28 and 29, which are the number of elements deleted vs. *x*/D for the three building types (13.4^0, 25.5^0 or 35.1^0 gable) when tested under same vane angle (Vane 1/ 15^0 vane angle), we can see that failure starts early on for cases which have slower tornado translational speed (TS = 15.0 m/s) than for cases with higher tornado translational speed (TS = 69.0 m/s). It can also be seen from Figures 27, 28 and 29, that for the slower moving tornados, the damage initiates at an *x*/D value of -4.934 for the 13.4^0 gable roof, -5.086 for the 25.5^0 gable roof and -5.543 for the 35.1^0 gable roof respectively. This shows that for a higher roof angle, the damage to the roof starts much early on when the tornado is further away from the center of the building. This is also seen for faster moving tornados as the damage initiates at an *x*/D value of -3.695 for the 13.4^0 gable roof, -3.847 for the 25.5^0 gable roof and -5.543 for the 35.1^0 gable roof respectively.

Comparing the same three figures, there seems to be a clear gap in-between the sets of slower and faster moving tornados of around 1.0 *x*/D. But when comparing the same building model (35.1^0 gable roof) with 3 different vane angles as in Figures 29, 30 and 31, the damage starts to rise at about the same *x*/D value. Also as mentioned earlier, the damage initiates closer to the center of the building for higher vane angles.

Similar to the tests conducted without the failure criteria, a set of 30 composite movie files were created. This shows the sequential damage as the tornado goes past the building. An example is shown in Figures 32 to 35 where the test was run for a 35.1^0 gable roofed building at 0^0 orientation with the oncoming tornado having a vane angle of 35^0 and a tornado translational speed of 15.0 m/s. Each frame in these four figures shows the elements that have failed till that load step. From the composite movies, it is generally noticed that for most

cases, the 2X4 joints at the four corners fail very early. Secondly, the plywood at the edges fails almost simultaneously. Lastly, the front and rear of the wall starts to disintegrate which happens as the rest of the roof fails. This last effect, which is the breaking up of the front and rear walls starting at the apex of the gable is mainly noticeable for the 35.1^0 gable roof building but not for the 13.4^0 or 25.5^0 gable roof building.

The ANSYS results file for each of the cases run with the failure criteria collects details of the deactivated elements, element types, their location and load-step when it fails. From this we can determine the number of failed elements in each element type and the respective order of failure. The type of elements deactivated with respect to *x*/D is plotted for each of the 30 runs with failure criteria (case 31 to 60) from Figures 36 to 65. It is seen that the 2X4s and the roof elements start failing at the same step for the majority of the cases. They are closely followed by the failure initiation of the nail elements. A few other cases have the roof elements failing first but the beam elements start failing immediately in the next step. There is no specific trend observed on the occurrence of the 2X4 or beam element at the start of the failure, but both the elements start failing together within a few steps of each other. Based on these results it can be said that irrespective of which element fails first, eventually the most failure occurs in the roof elements.

CHAPTER 6. CONCLUSION AND FUTURE WORK

6.1 CONCLUSION

Full-scale numerical Finite Element models of gable roof buildings with three different roof angles (13.4^0, 25.5^0 and 35.1^0) were developed. The tornado induced wind loads recorded by the experimental procedure were applied on the model and the resulting stress distribution was studied. Also a routine in ANSYS was developed to incorporate a failure criterion for the building models. The damage sequence and damage intensity have been studied to estimate the debris formation. The following conclusions were made from the results,

1. Buildings that experience tornado forces with smaller swirl ratio (0.08) have higher peak stresses than those that experience tornado forces with higher swirl ratio (0.24, 1.14).
2. The peak stresses encountered by the 25.5^0 gable roof in all cases is the maximum. This is more than the 13.4^0 gable roof, which is more than what is encountered by the 35.1^0 gable roof.
3. Maximum stresses occur on the sides, at the junctions where the roof meets the walls (eaves) and at the top (ridge), where the two halves of the roofs meet.
4. There is also high stress concentration about half way between the roof edge and the roof center (ridge) which is at $1/4^{th}$ the total length of the roof. This high stress decreases with increase in roof angle.
5. As the roof angle increases, the gable area increases and the pressure on the roof increase. This results in an increase in stresses.

6. Failure starts early on for cases which have slower tornado translational speed (TS = 15.0 m/s) than for cases with higher tornado translational speed (TS = 69.0 m/s).
7. For a higher roof angle, the damage to the roof starts much early on even when the tornado is further away from the center of the building.
8. From the composite movies, it is generally noticed that for most cases, the 2X4 joints at the four corners (vertical corners) fail very early.
9. Once the 2X4s fail, the plywood at the edges fails almost simultaneously.
10. Lastly, the front and rear of the wall starts to disintegrate which happens as the rest of the roof fails.
11. The breaking up of the front and rear walls starting at the apex of the gable is mainly noticeable for the 35.1^0 gable roof building but not for the 13.4^0 or 25.5^0 gable roof building.
12. There is no specific trend observed on the occurrence of the 2X4 or nail element at the start of the failure, but both the elements start failing together within a few steps of each other.
13. Irrespective of which type of element fails first, the roof panels sustain the maximum failure.

6.2 FUTURE WORK

1. Three types of buildings were tested. The ANSYS code can easily be modified to various other types of buildings like hipped roof, flat roof, etc.

2. Multi-storied buildings can be studied.
3. In reality, the roof elements have a plate to join the gable to the base but this research has used nail elements. The properties of the plate elements can be studied and used for further analysis.
4. The frame 2X4 spacing can be optimized to reduce failure.
5. Stiffened members in certain areas can be employed to reduce failure.

CHAPTER 7. TABLES

Case Name	Vane Angle (deg)	Fan Speed (%FS)	Floor Height (m)	S at RMW	RMW (m)	$V_{\theta_{max}}$ (m/s)	Q (m^3/s)	λ_T	Re $\times 10^4$
Vane1	15	0.33	0.46	0.08	0.23	6.9	14.4	10.4	4.3
Vane2	25	0.33	0.46	0.18	0.30	8.3	13.1	12.5	5.1
Vane3	35	0.33	0.46	0.24	0.30	9.7	11.5	14.7	6.0
Vane4	45	0.33	0.46	0.82	0.51	9.8	9.7	14.9	6.1
Vane5	55	0.33	0.46	1.14	0.53	9.7	7.6	14.8	6.0

Table 1. Experimental simulator settings and the accompanying tornado vortex parameters. S=Swirl Ratio, RMW = Radius of Maximum Wind, Q = Volume Flow Rate, λ_T = Time Scale, Re = Model Reynolds No.

Vane	$V_{\theta m}$ m/s	$V_{\theta fs}$ m/s	λ_V	λ_T	τ_{fs}	Conversion factor
1	6.9	50.5	1:7.3	01:13.8	358.8	53.57
2	8.3	50.2	1:6.0	01:16.5	429	36.58
3	9.7	49.8	1:5.1	01:19.4	504.4	26.36
4	9.8	49.8	1:5.1	01:19.6	509.6	25.82
5	9.7	49.8	1:5.1	01:19.6	509.6	26.36

Table 2. Table showing the Pressure conversion factor. V_θ: Maximum tangential velocity, λ_V: Velocity ratio, λ_T: Time Ratio, t: Time, m: model, fs: full-scale.

Building model	Building Type	Roof Angle Θ
1	Residential 1 Story	13.4
2	Residential 1 Story	25.5
3	Residential 1 Story	35.1

Table 3. Building types tested.

Vane	Vane angle	Crane Speed - model		Tornado TS - full scale	
		m/s	ft/s	m/s	ft/s
Vane 1	15	0.1524	0.5	15.24	50.0
		0.6096	2	60.96	200.0
Vane 3	35	0.1524	0.5	15.24	50.0
		0.6096	2	60.96	200.0
Vane 5	55	0.1524	0.5	15.24	50.0
		0.6096	2	60.96	200.0

Table 4. Conversion of crane translational speed in lab to full-scale tornado translational speed for different vane angles used.

Without Failure Criteria										
Bldg. angle	**Model 1**		**Model 2**		**Model 3**					
	Vane 1		**Vane 1**		**Vane 1**		**Vane 3**		**Vane 5**	
TS ->	**15 m/s**	**61 m/s**	**15 m/s**	**61 m/s**	**15 m/s**	**61 m/s**	**15 m/s**	**61 m/s**	**15 m/s**	**61 m/s**
0	*1*	*4*	*7*	*10*	*13*	*16*	*19*	*22*	*25*	*28*
45	*2*	*5*	*8*	*11*	*14*	*17*	*20*	*23*	*26*	*29*
90	*3*	*6*	*9*	*12*	*15*	*18*	*21*	*24*	*27*	*30*

Table 5. Test matrix for Analysis with and without failure criteria, TS: Tornado Translational Speed.

With Failure Criteria										
Bldg.	Model 1		Model 2		Model 3					
angle	Vane 1		Vane 1		Vane 1		Vane 3		Vane 5	
TS ->	15 m/s	61 m/s	15 m/s	61 m/s	15 m/s	61 m/s	15 m/s	61 m/s	15 m/s	61 m/s
0	*31*	*34*	*37*	*40*	*43*	*46*	*49*	*52*	*55*	*58*
45	*32*	*35*	*38*	*41*	*44*	*47*	*50*	*53*	*56*	*59*
90	*33*	*36*	*39*	*42*	*45*	*48*	*51*	*54*	*57*	*60*

Table 6. Test matrix for Analysis with and with failure criteria, TS: Tornado Translational Speed.

CHAPTER 8. FIGURES

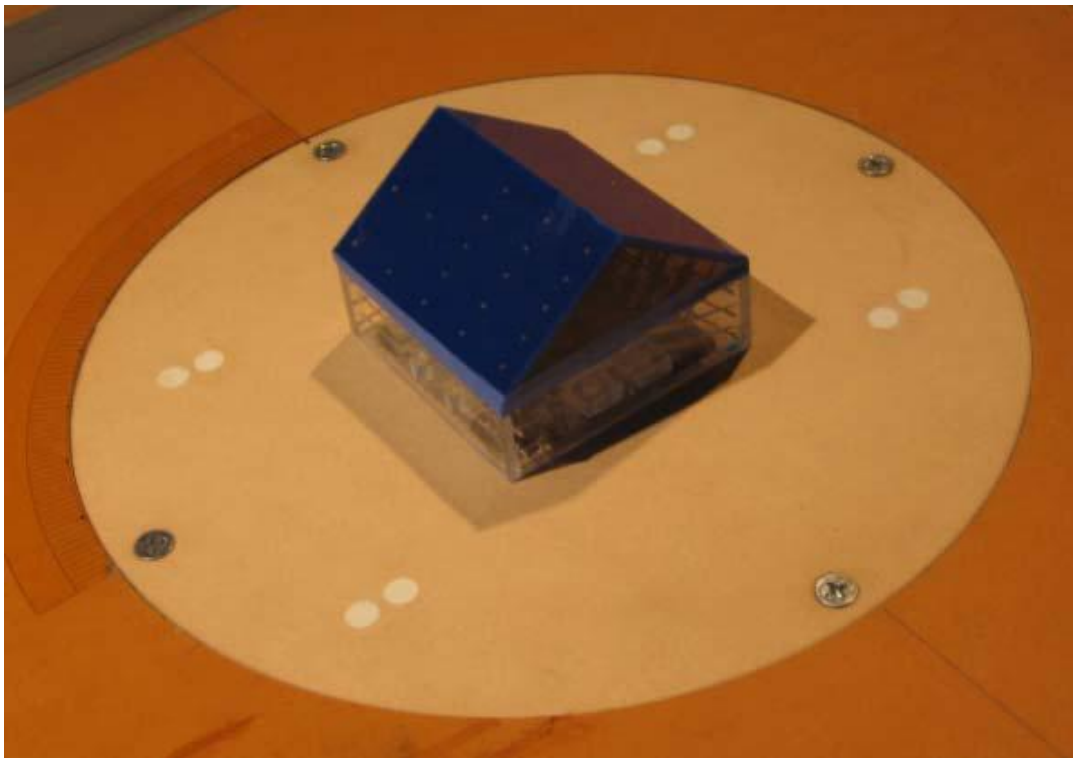

Figure 1. Photo of gable roof building model with pressure taps.

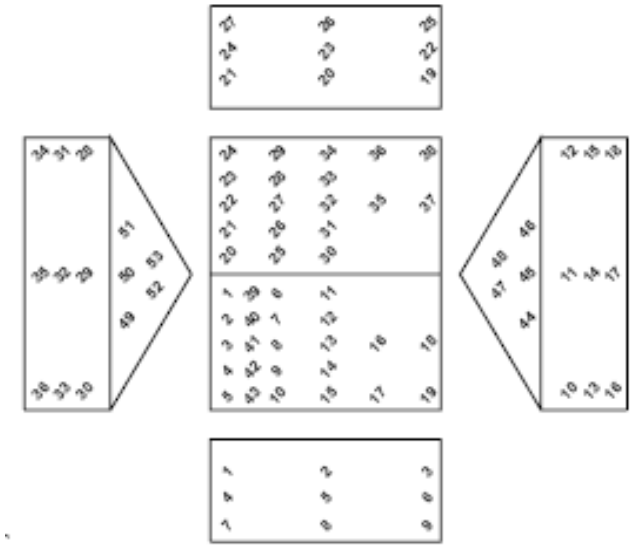

Figure 2. Exploded view of the gable roof building with pressure tap labels.

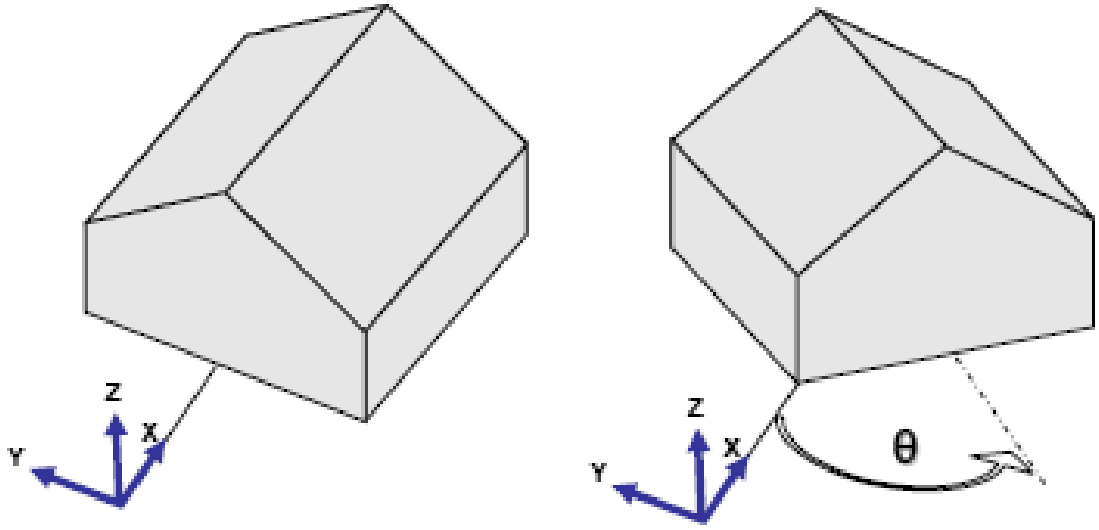

Figure 3. Building orientation with respect to the vortex translation direction (*x*-axis)

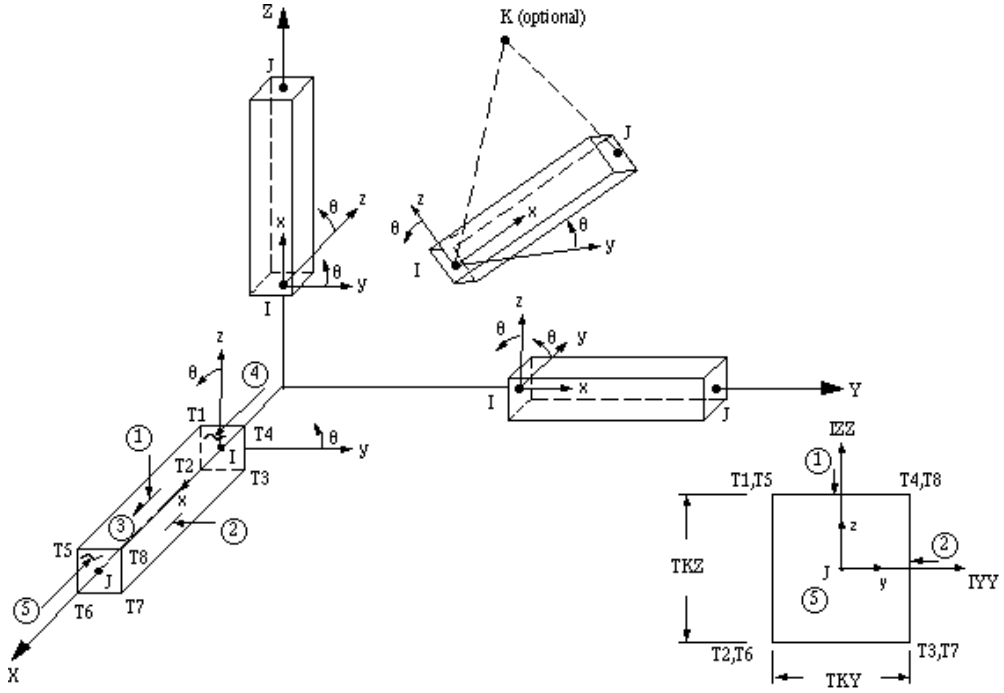

Figure 4. BEAM4 3-D Elastic Beam

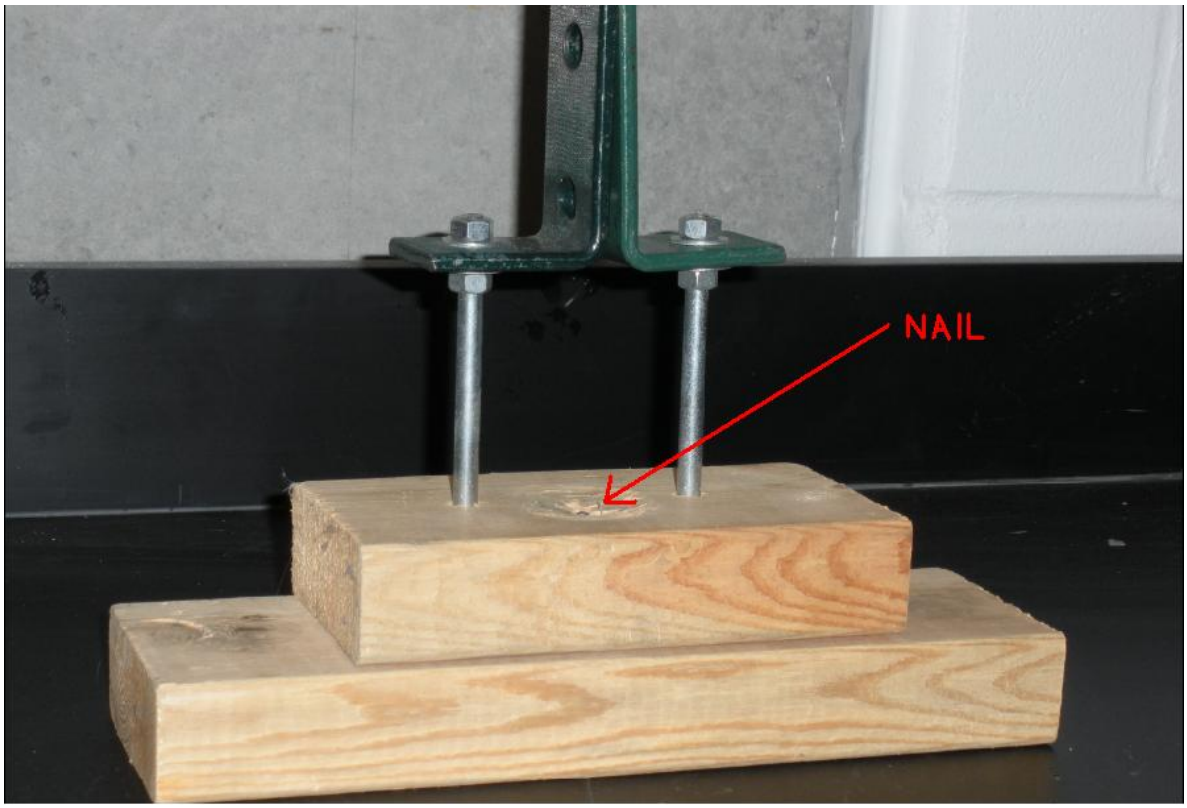

Figure 5. Nail Pull test showing the two 2X4s and nail location.

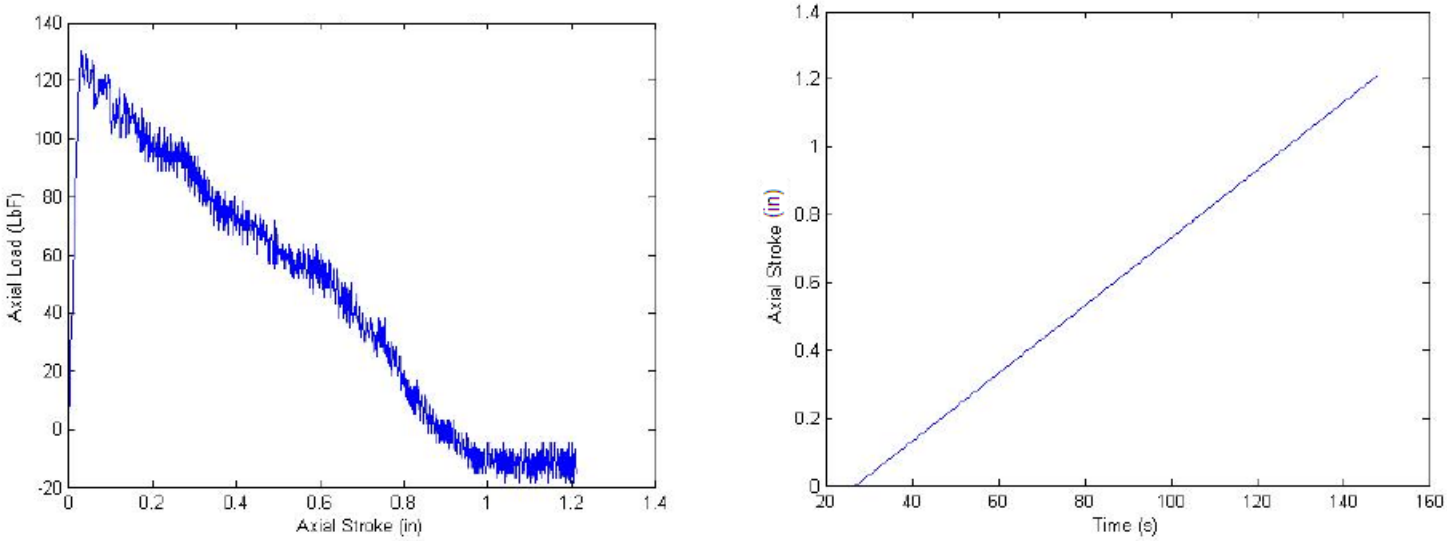

Figure 6. (a) Axial load (LbF) vs. Axial stroke (in) as the nail is pulled out of the wood, and (b) Axial stroke (in) as a function of time(s) for the test.

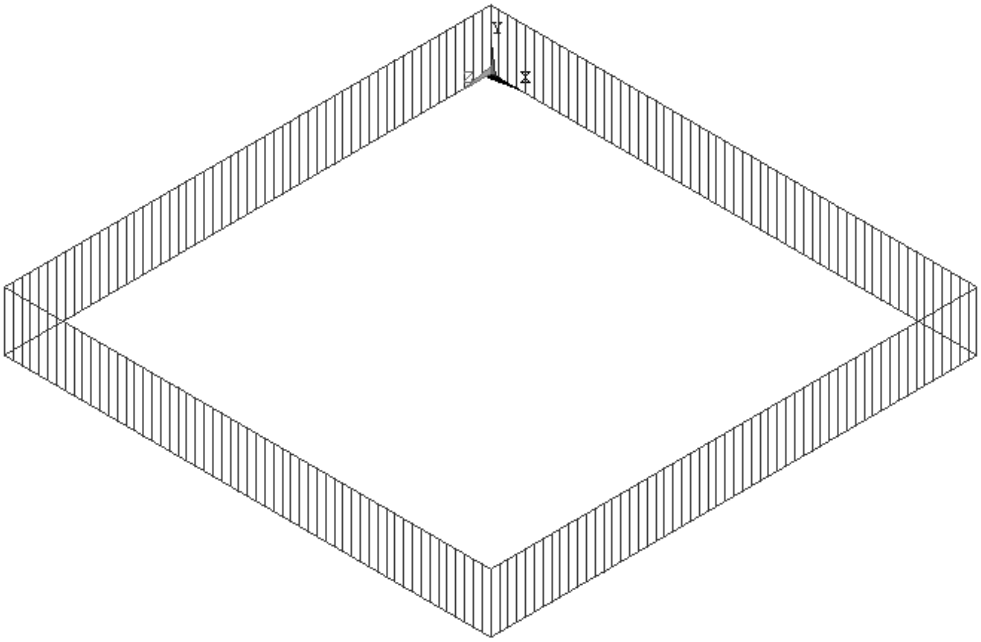

Figure 7. Wall framework of 2X4s

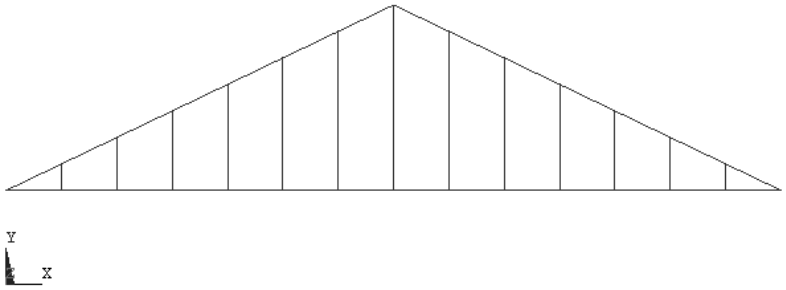

Figure 8. Gable roof assembly, Front view.

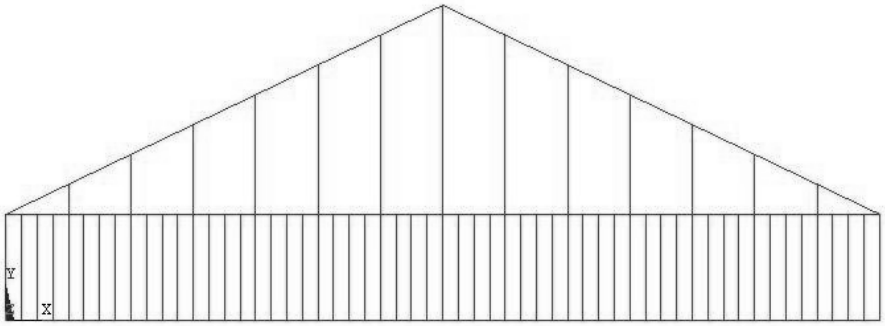

Figure 9. 2X4 framework assembly, Front view.

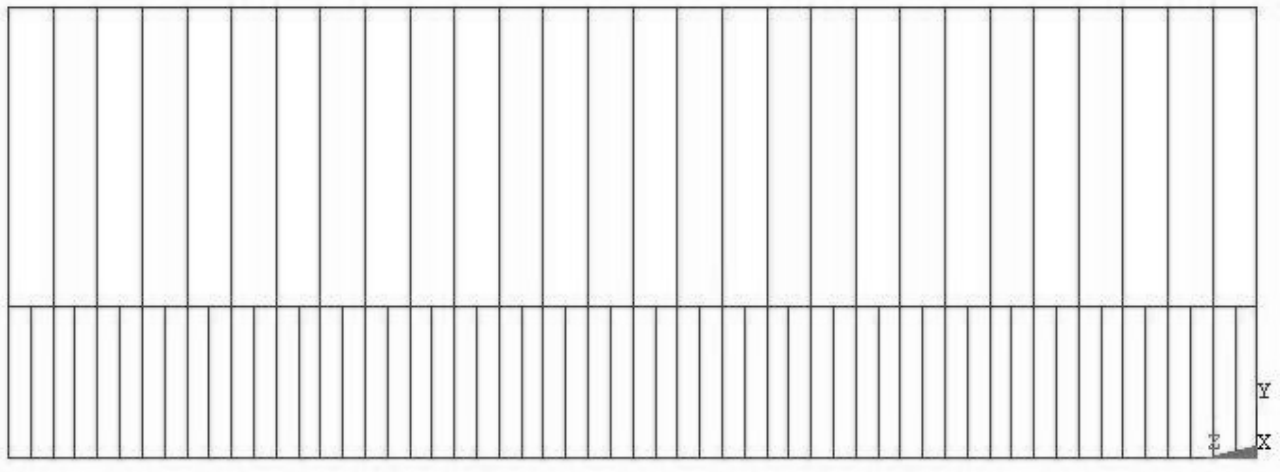

Figure 10. 2X4 framework assembly, Side view.

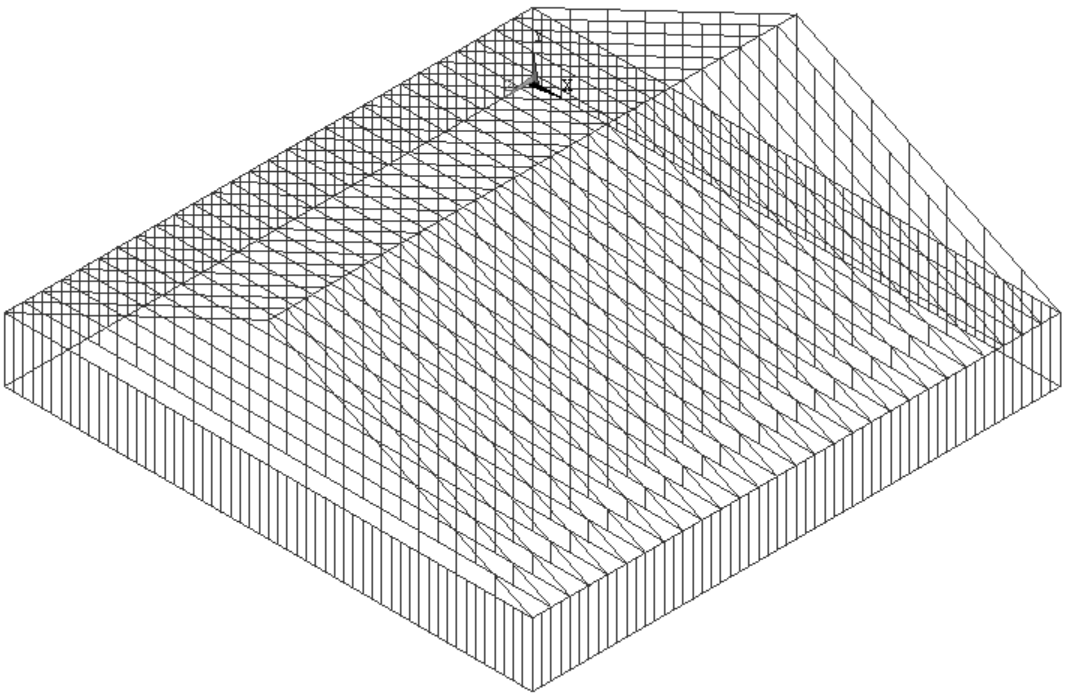

Figure 11. 2X4 framework assembly, Isometric view.

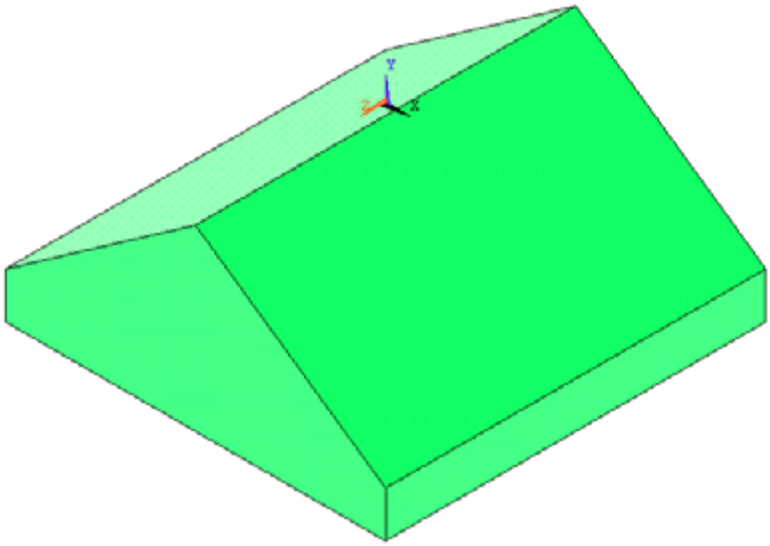

Figure 12. Area plot over frame before meshing.

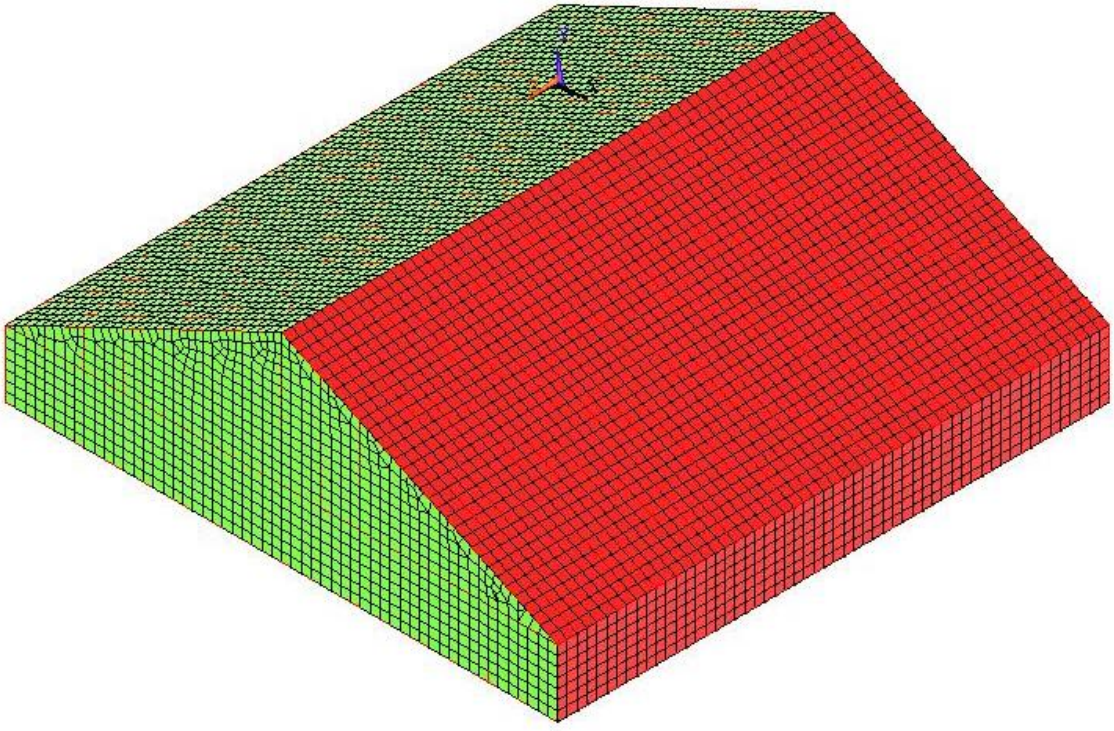

Figure 13. Model exterior after meshing, Isometric view.

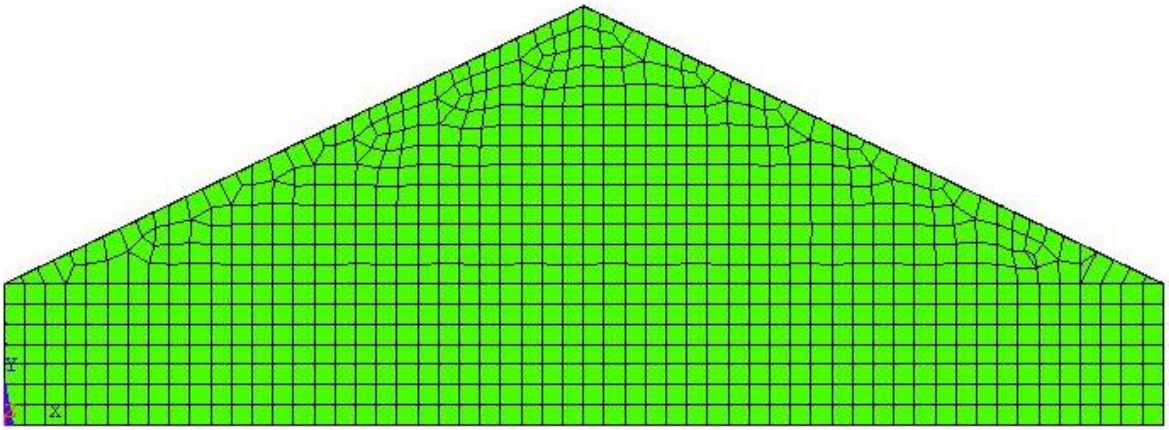

Figure 14. Model exterior after meshing, Front view.

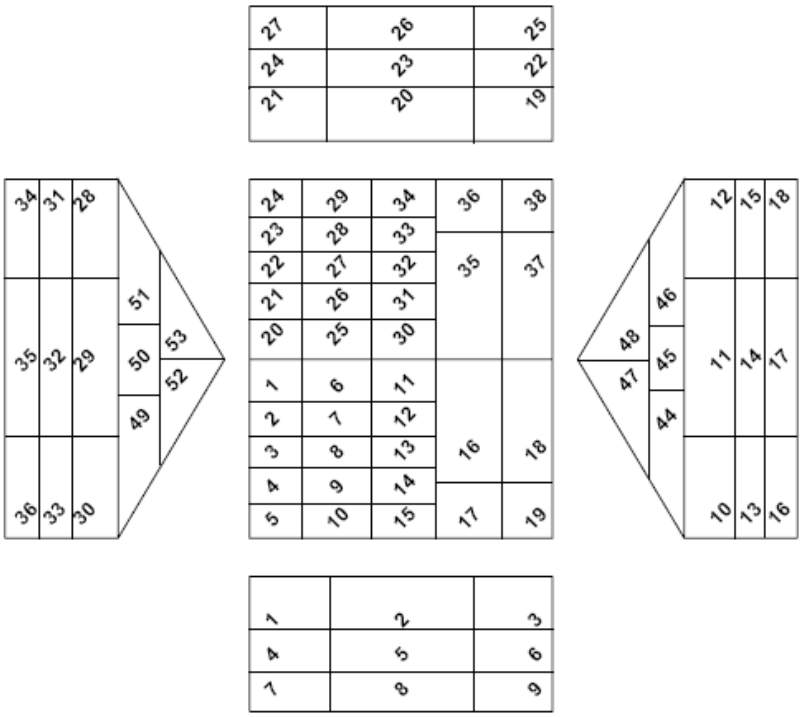

Figure 15. Approximating the area around the pressure tap to have the same pressure value.

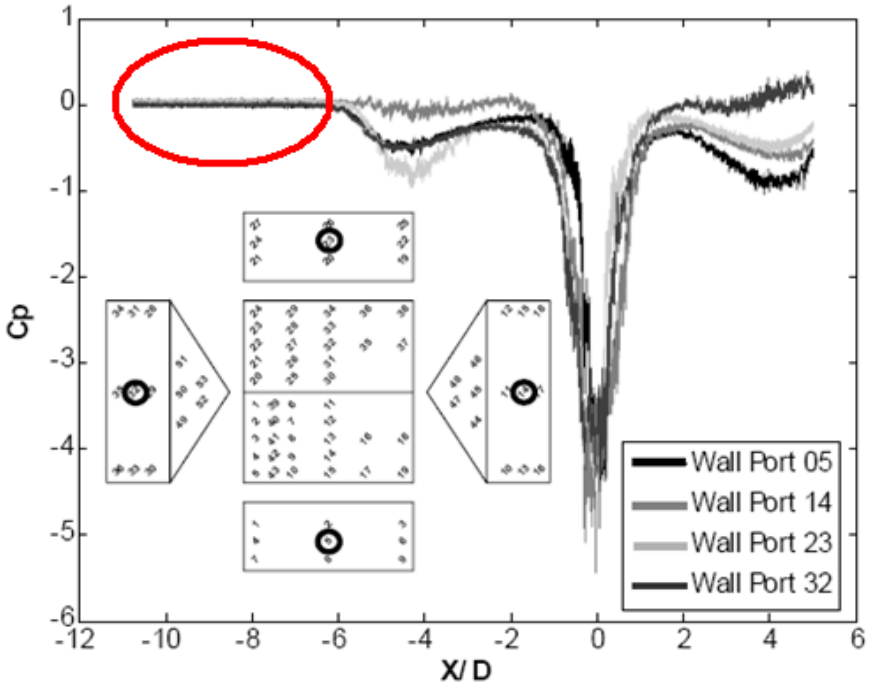

Figure 16. *Cp* time history at Wall Port # 5, 14, 23& 32 for a 35.1^0 gable roof building at 0^0 building orientation, crane speed 5ft/s and 15^0 vane angle.

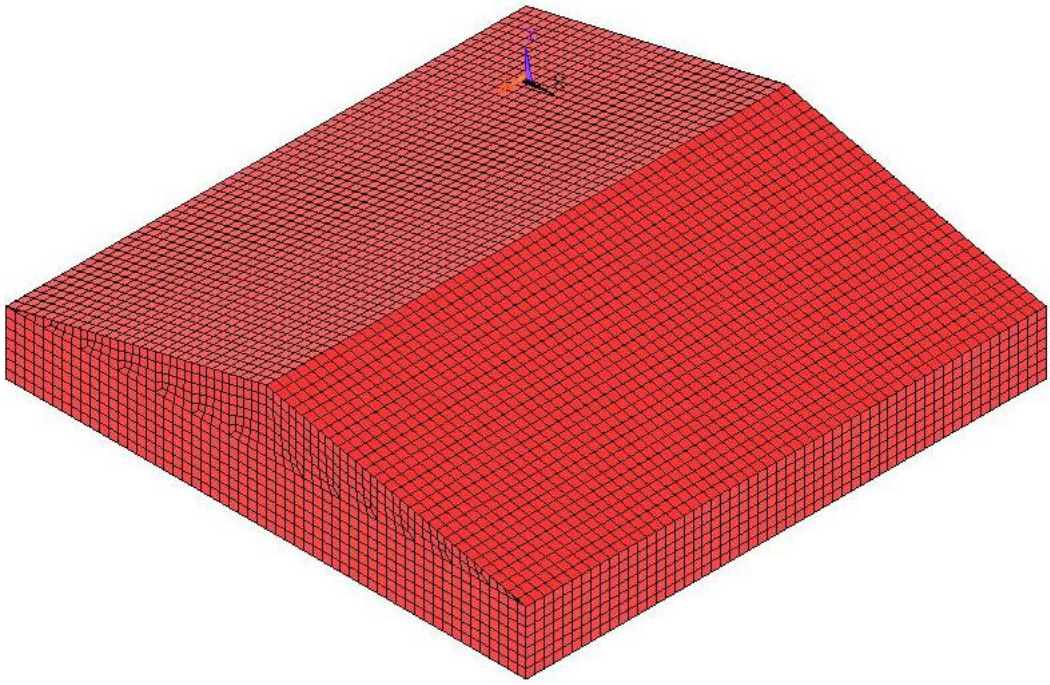

Figure 17. 1 Story Gable Roof with $\theta = 13.4^0$ Model

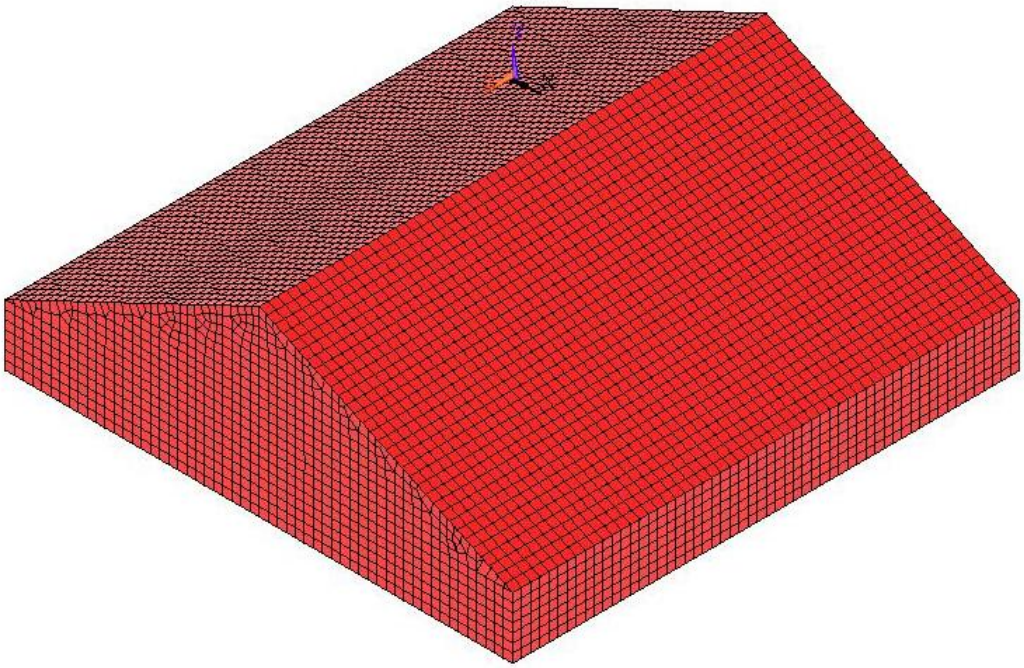

Figure 18. 1 Story Gable Roof with $\theta = 25.5^0$ Model

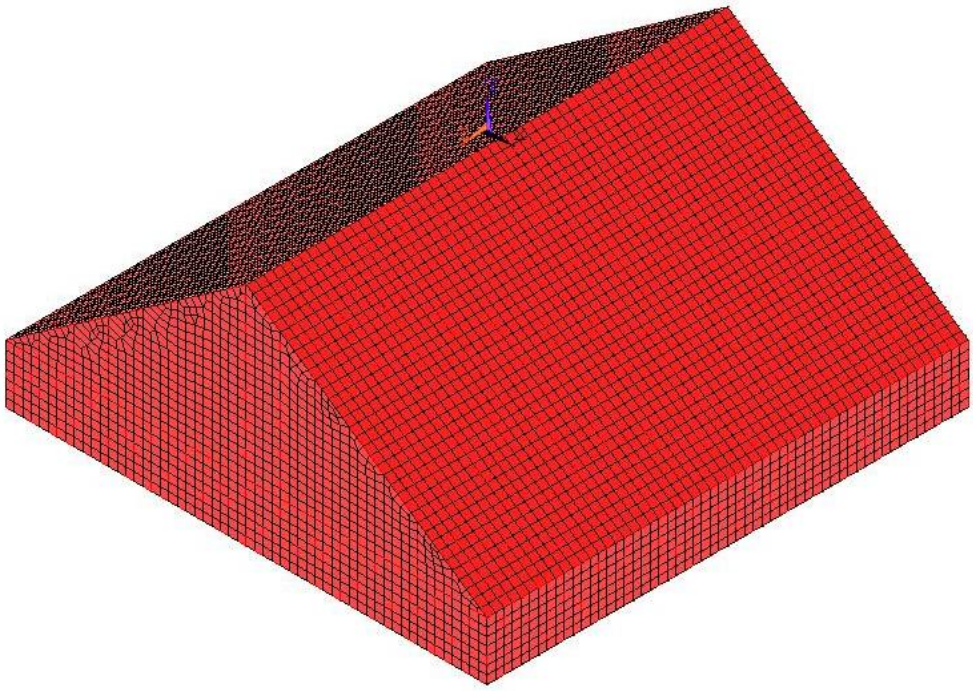

Figure 19. 1 Story Gable Roof with $\theta = 35.1^0$ Model

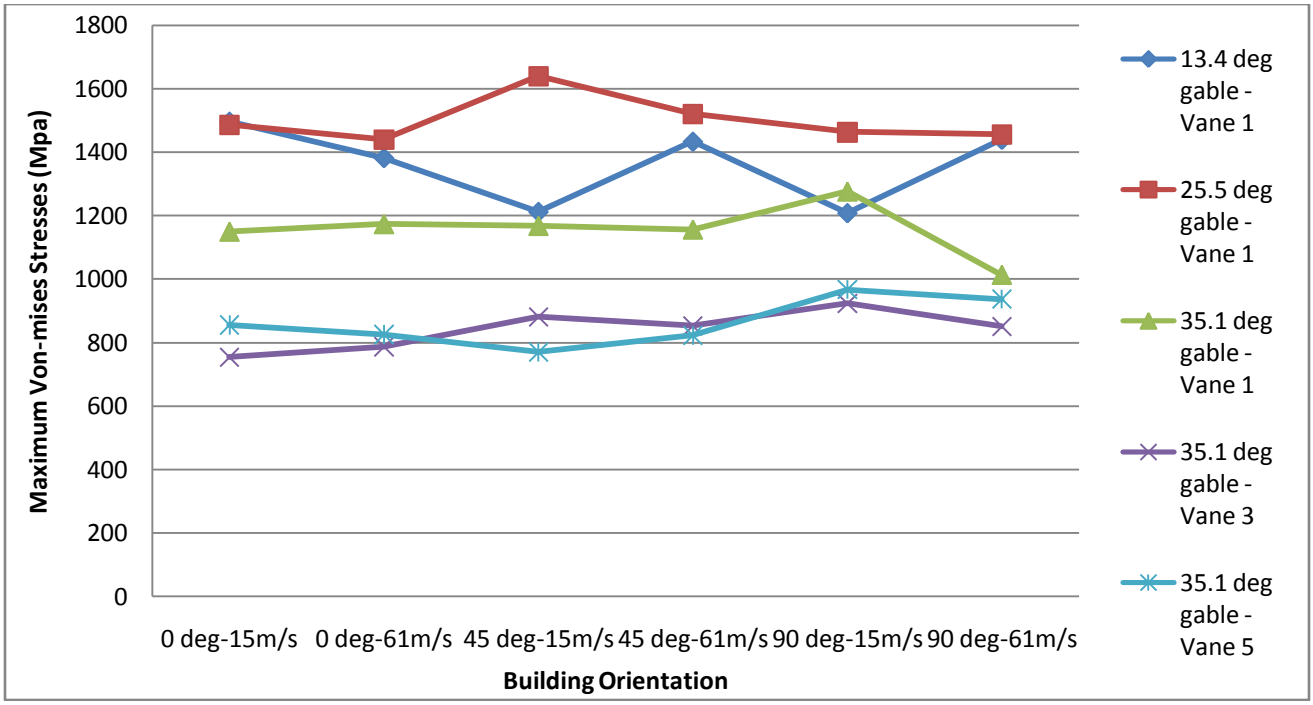

Figure 20. Maximum Von-mises stresses vs. Building orientation for all cases (Tornado translational speeds are mentioned near markers).

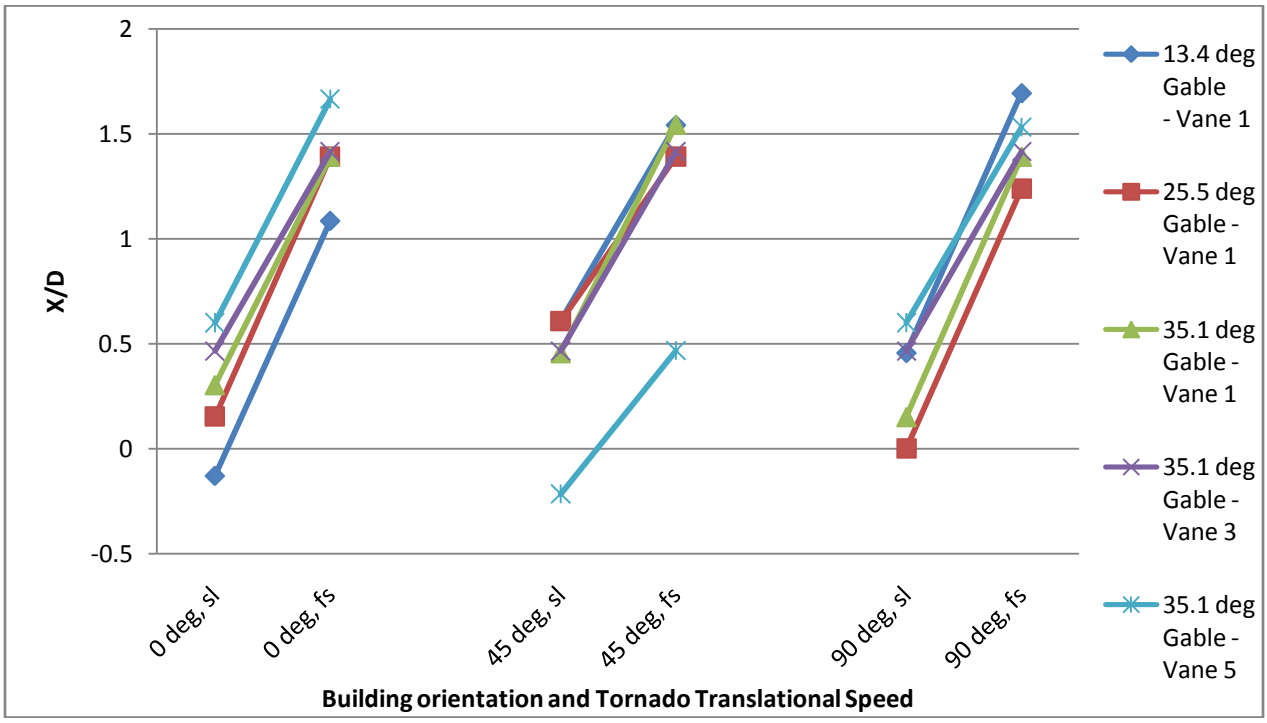

Figure 21. Location of tornado with respect to building vs. Test case

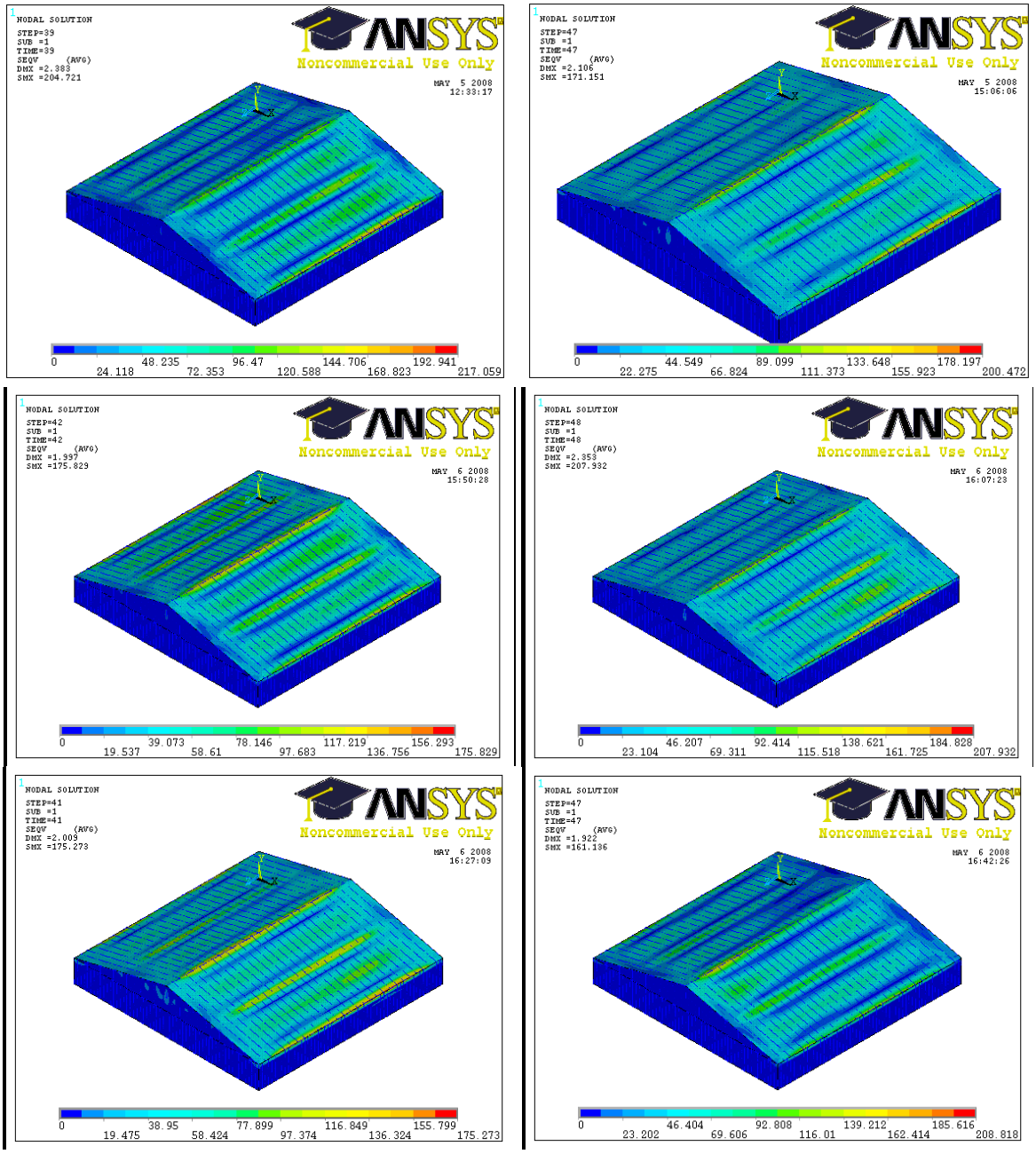

Figure 22. Snapshot of cases 1 to 6 (13.4^0 gable roof with 15^0 vane angle (Vane 1)) showing stage of peak stress distribution (counter clockwise starting from top left image).

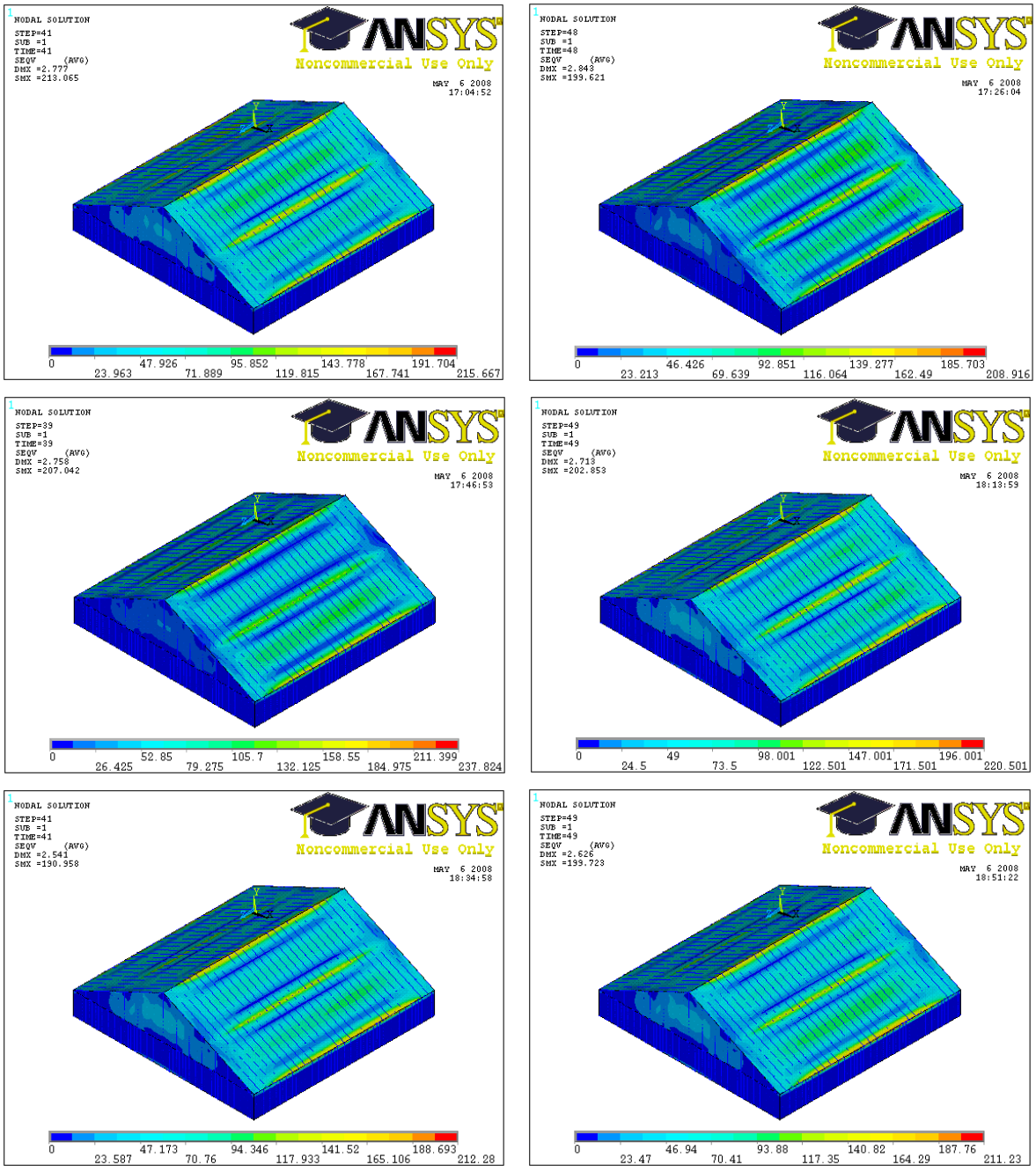

Figure 23. Snapshot of cases 7 to 12 (25.5^0 gable roof with 15^0 vane angle (Vane 1)) showing stage of peak stress distribution (counter clockwise starting from top left image).

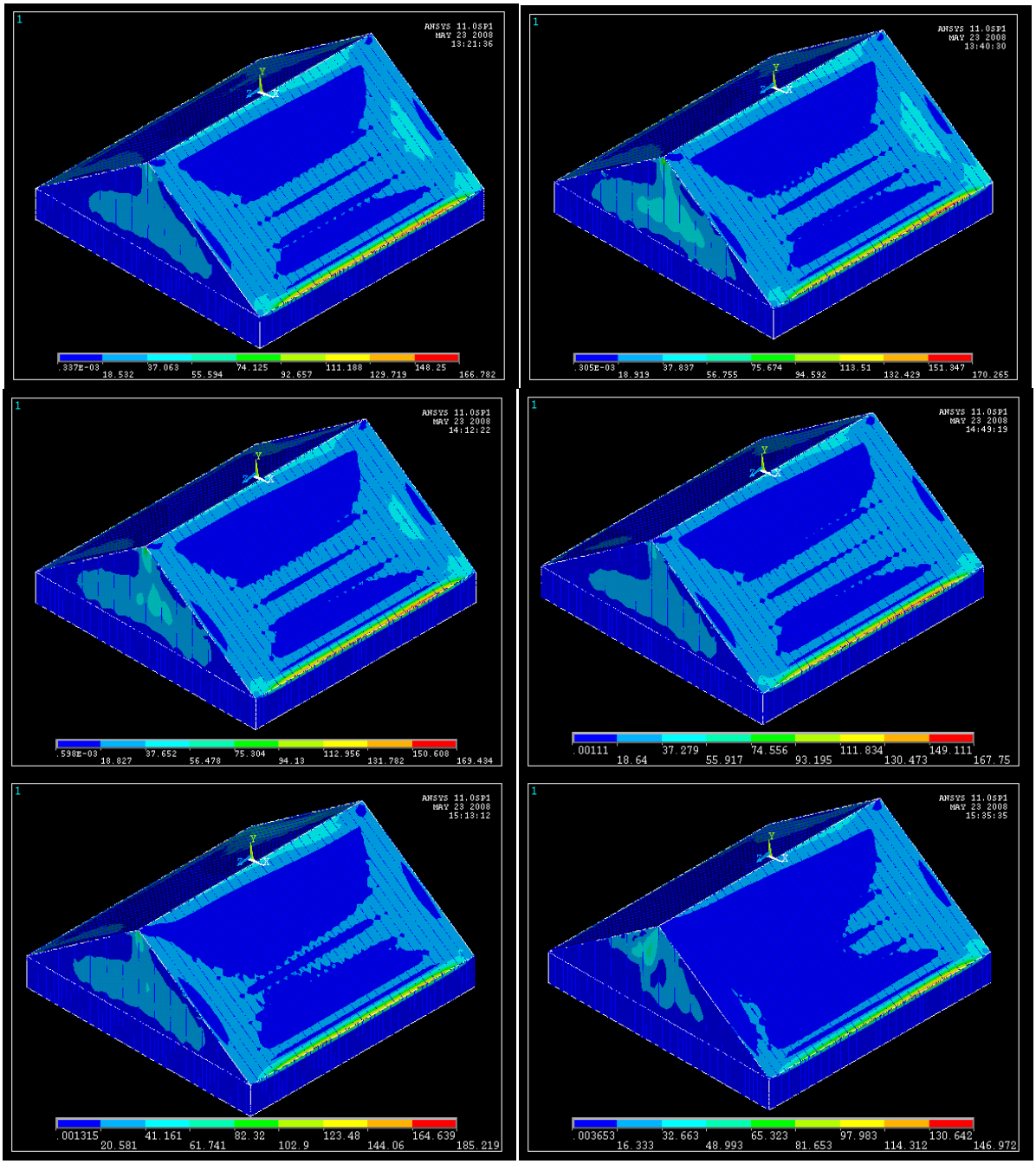

Figure 24. Snapshot of cases 13 to 18 (35.1^0 gable roof with 15^0 vane angle (Vane 1)) showing stage of peak stress distribution (counter clockwise starting from top left image).

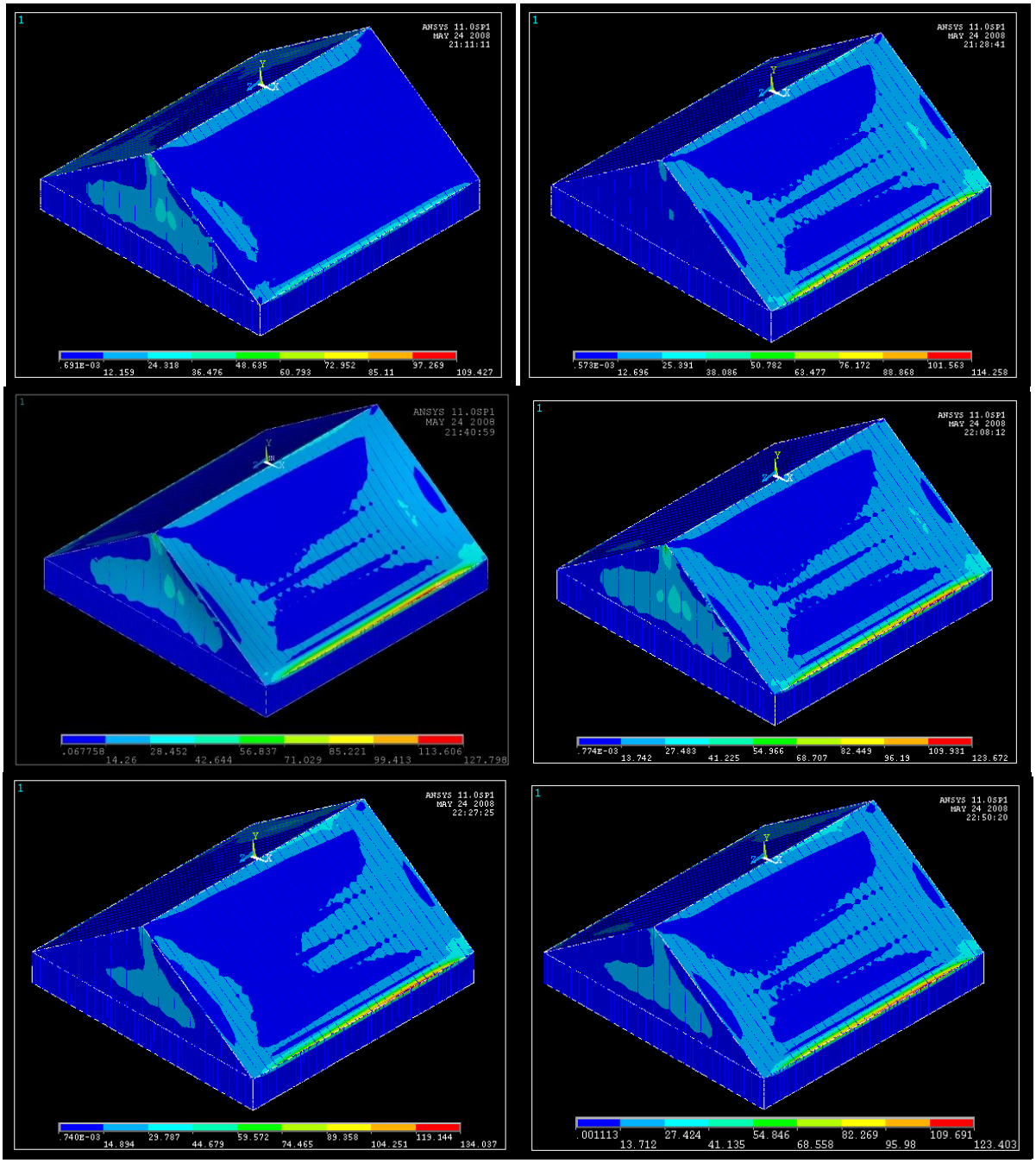

Figure 25. Snapshot of cases 19 to 24 (35.1^0 gable roof with 35^0 vane angle (Vane 3)) showing stage of peak stress distribution (counter clockwise starting from top left image).

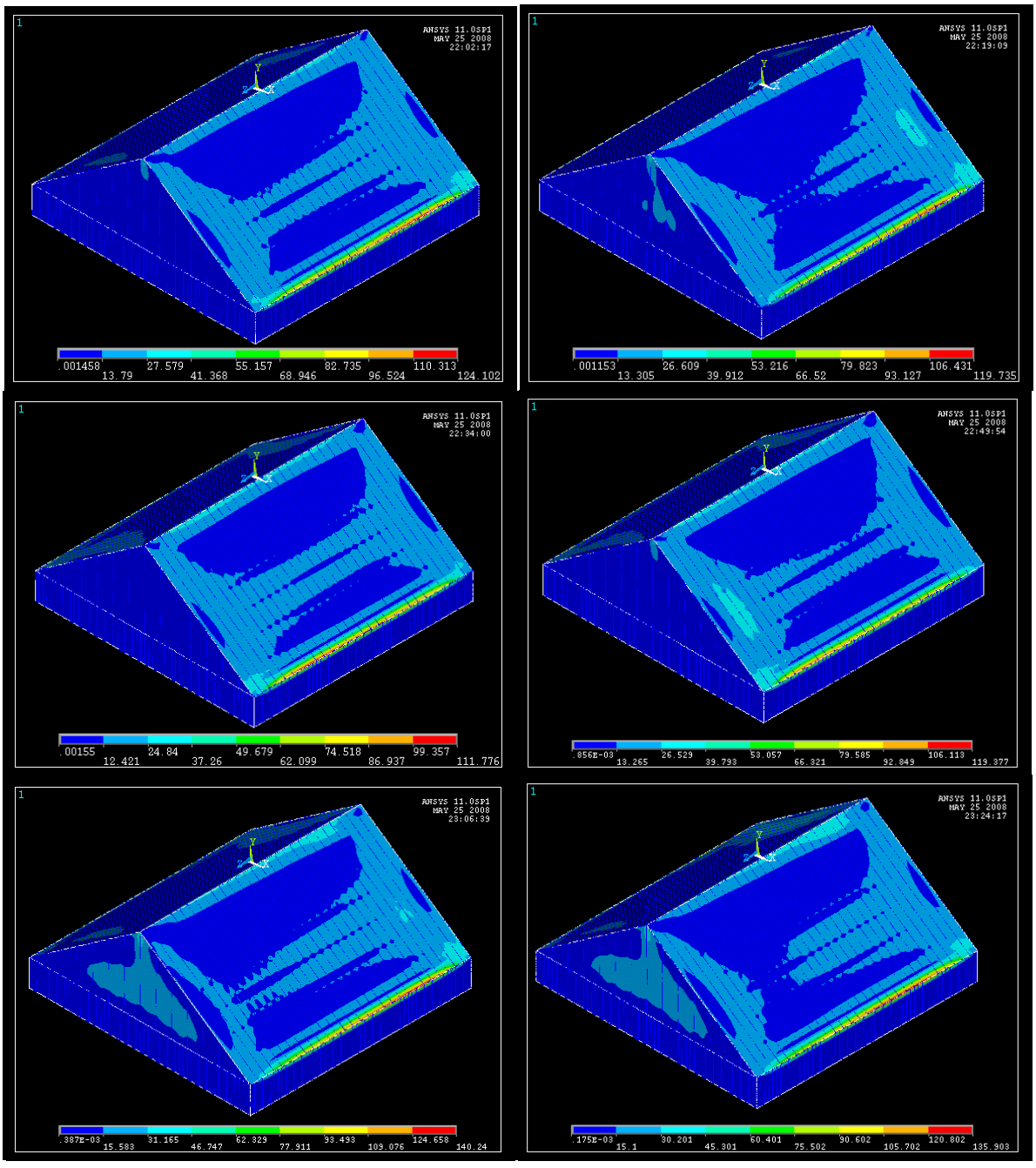

Figure 26. Snapshot of cases 25 to 30 (35.1^0 gable roof with 55^0 vane angle (Vane 5)) showing stage of peak stress distribution (counter clockwise starting from top left image).

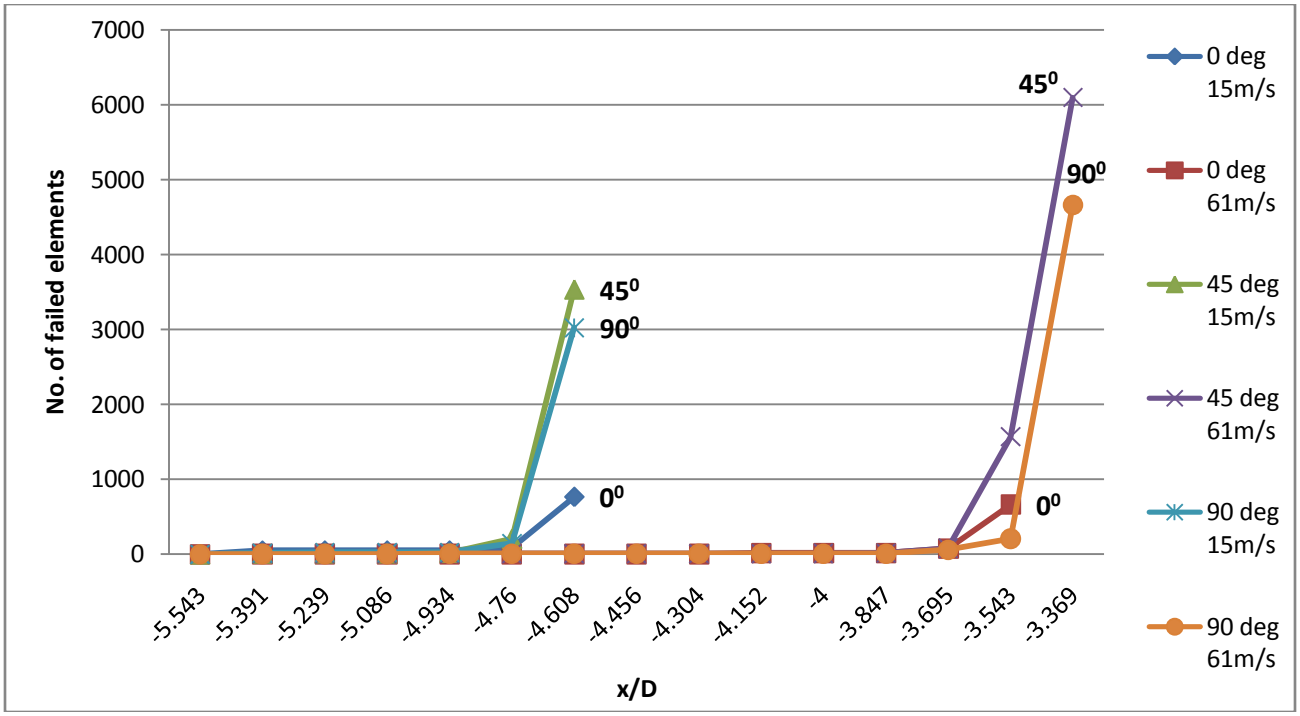

Figure 27. Total number of failed elements vs. X/D for 13.4^0 gable roof, 15^0 vane angle.

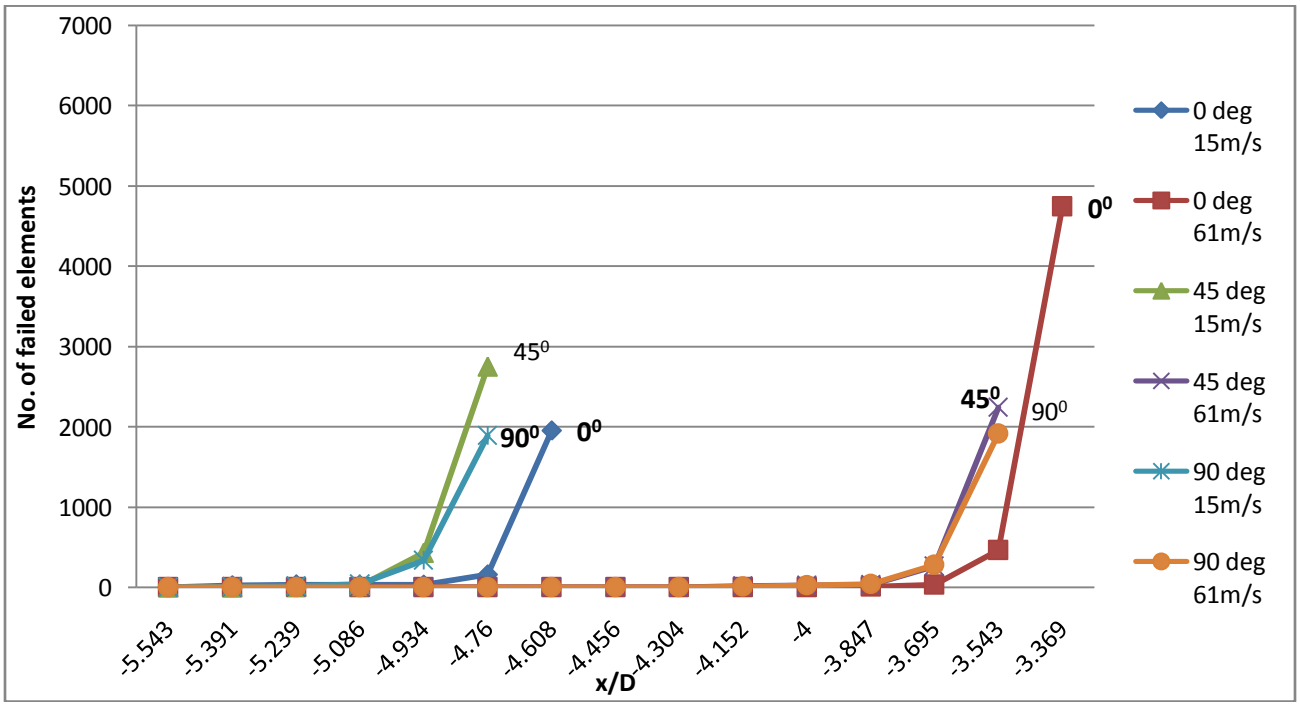

Figure 28. Total number of failed elements vs. X/D for 25.5^0 gable roof, 15^0 vane angle.

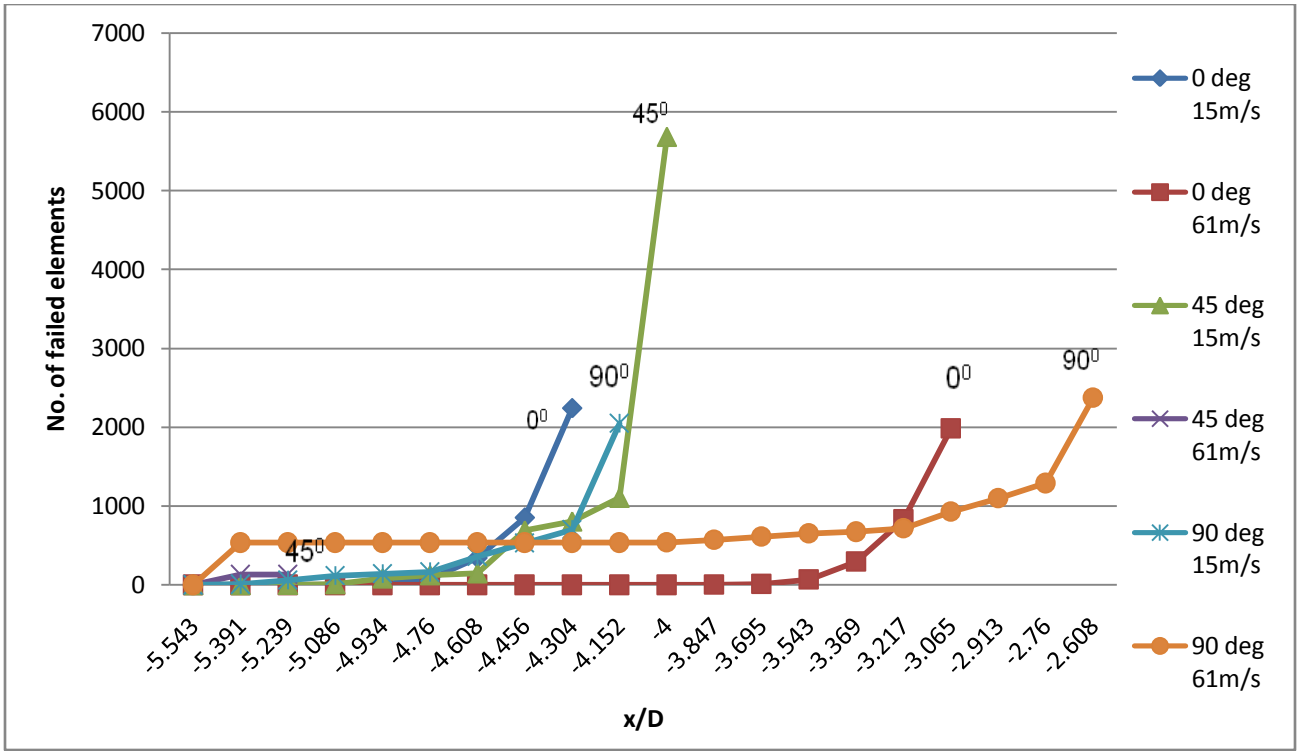

Figure 29. Total number of failed elements vs. X/D for 35.1^0 gable roof, 15^0 vane angle.

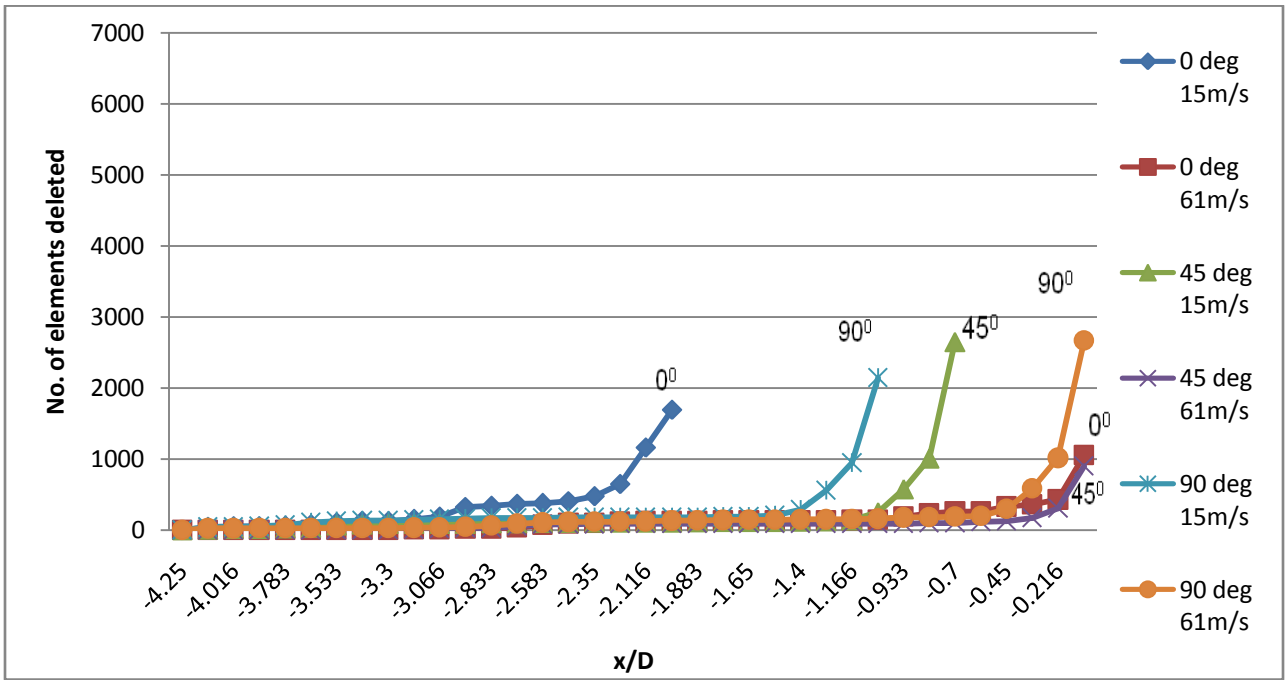

Figure 30. Total number of failed elements vs. X/D for 35.1^0 gable roof, 35^0 vane angle.

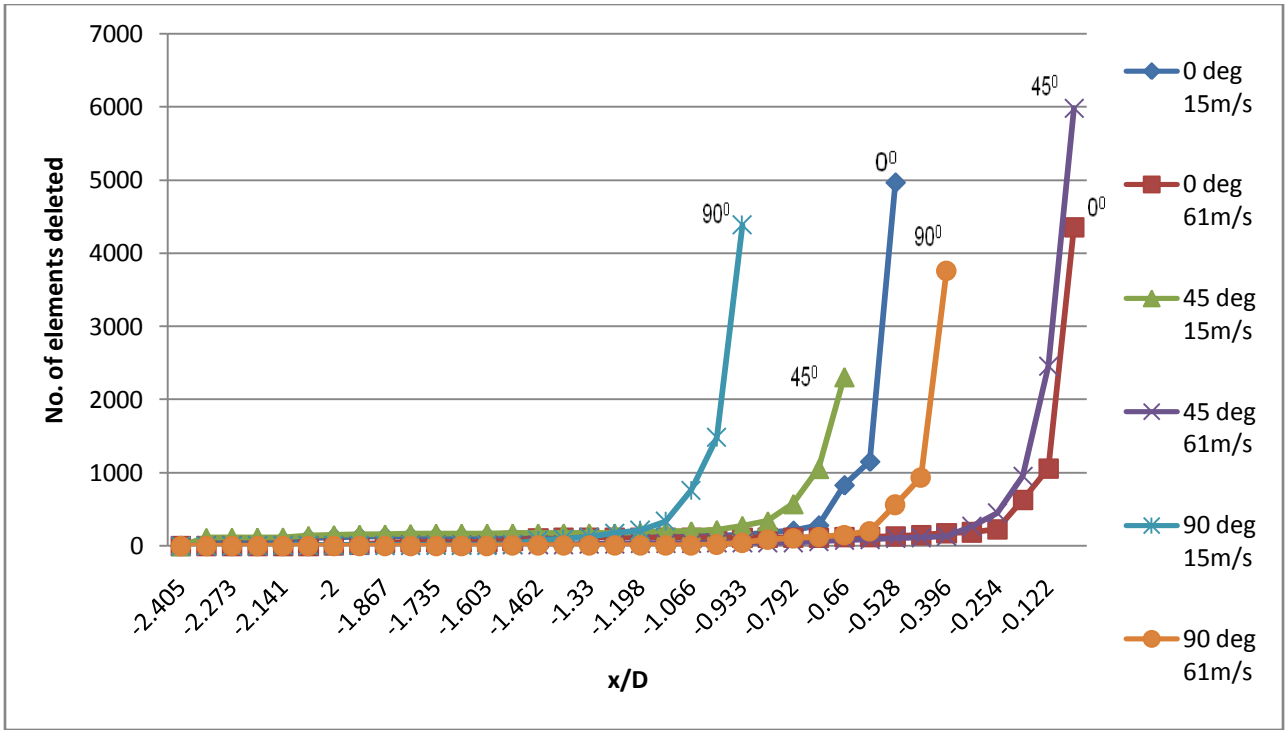

Figure 31. Total number of failed elements vs. X/D for 35.1^0 gable roof, 55^0 vane angle.

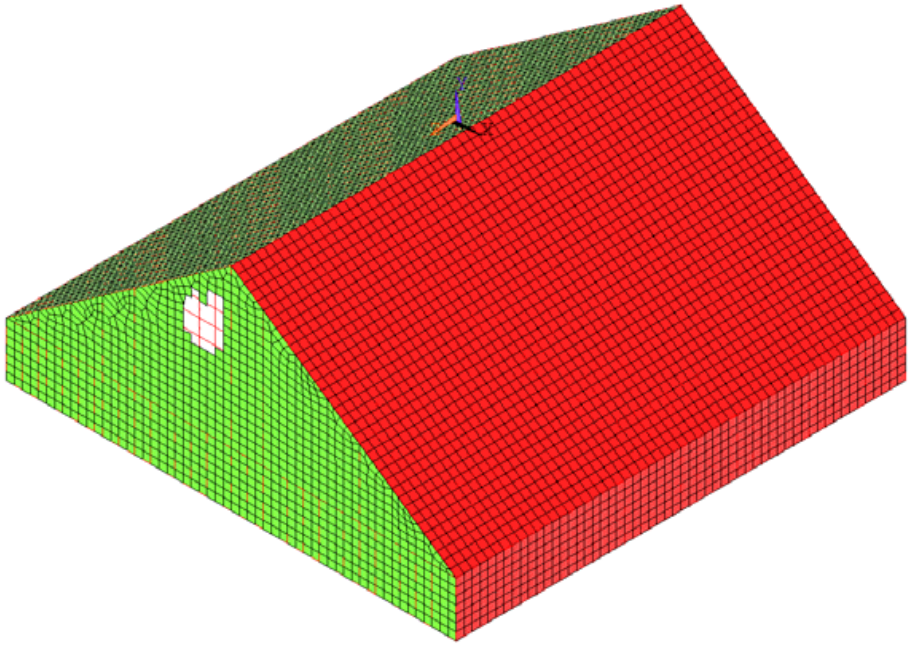

Figure 32. Snapshot of elements deleted (or failed) for example case no: 49 at *x*/D = -4.76. 47 Elements deleted.

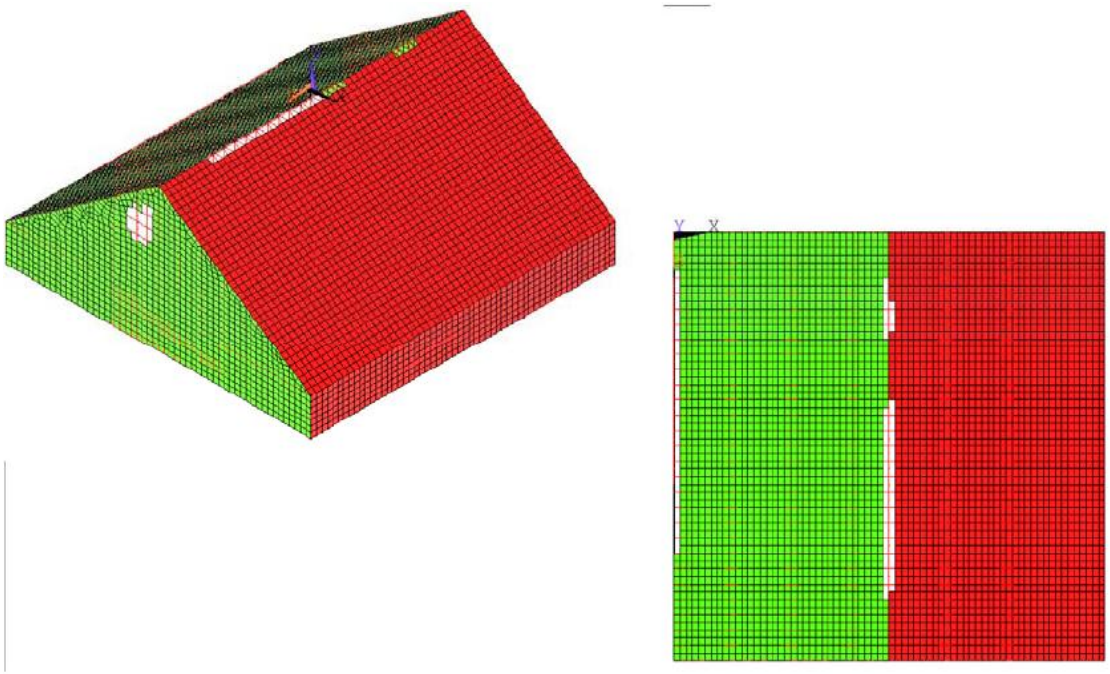

Figure 33. Snapshot of elements deleted (or failed) for example case no: 49 at *x*/D = -4.608. 181 Elements deleted, Isometric and Top view.

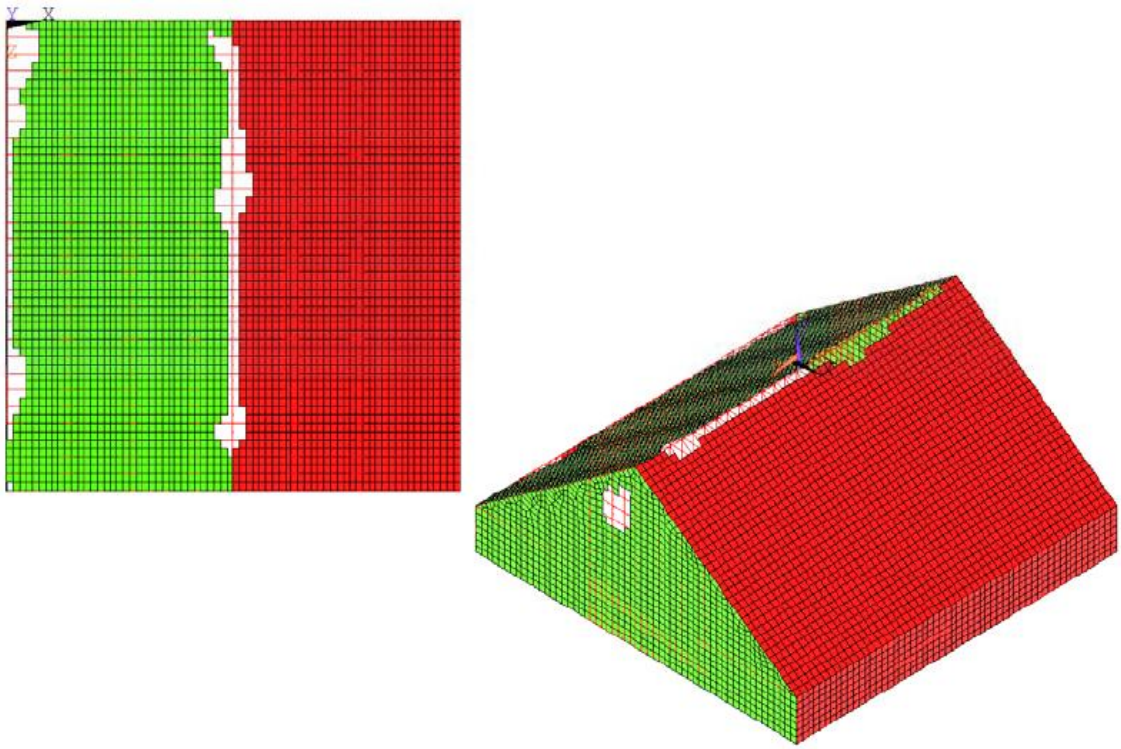

Figure 34. Snapshot of elements deleted (or failed) for example case no: 49 at *x*/D = -4.456. 383 Elements deleted, Top and Isometric view.

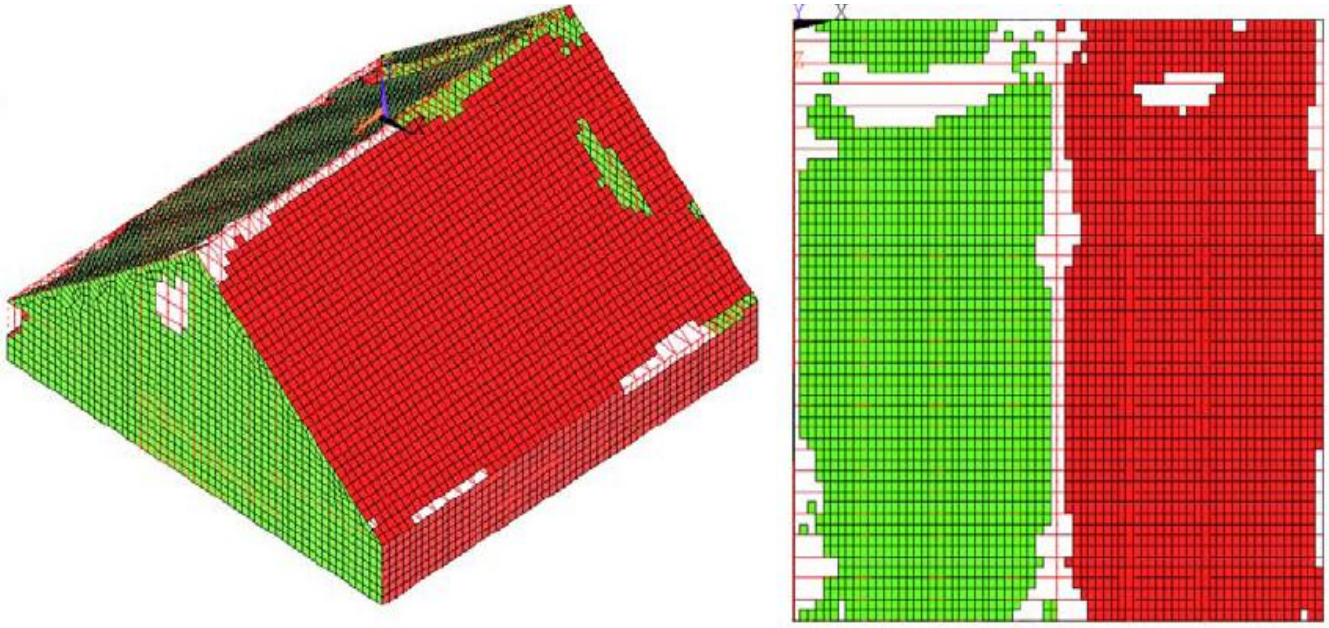

Figure 35. Snapshot of elements deleted (or failed) for example case no: 49 at *x*/D = -4.152. 861 Elements deleted, Isometric and Top view.

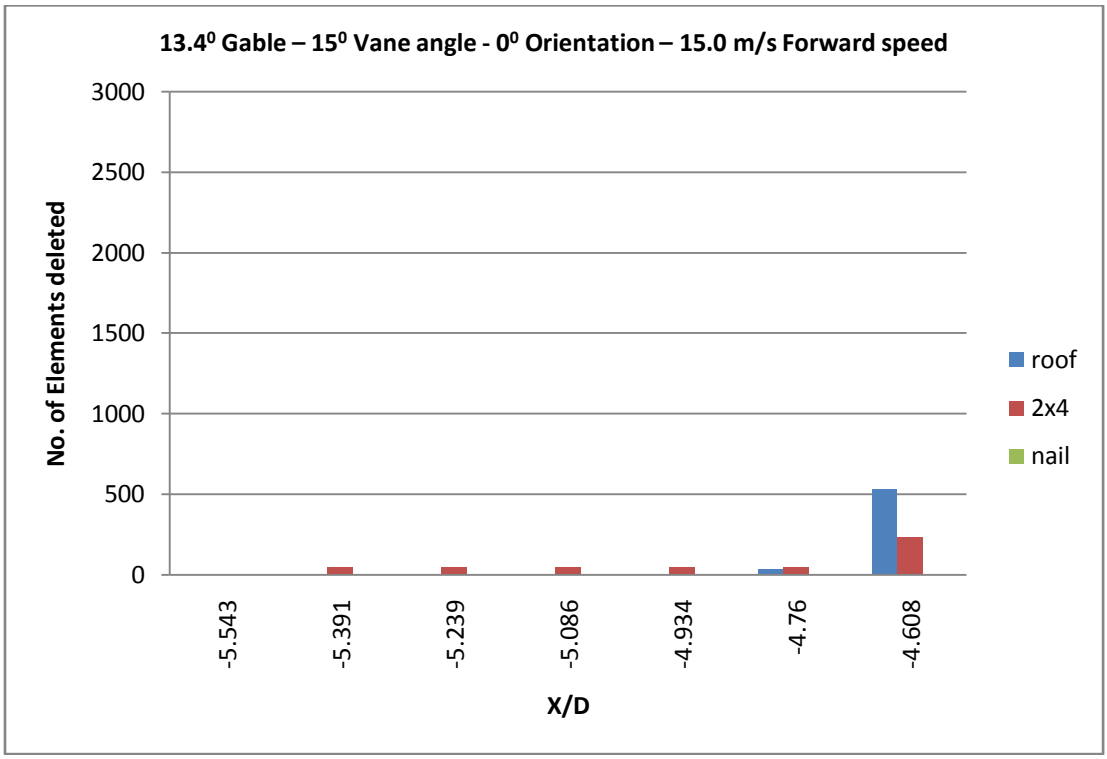

Figure 36. Number of elements failed vs. X/D for case 31

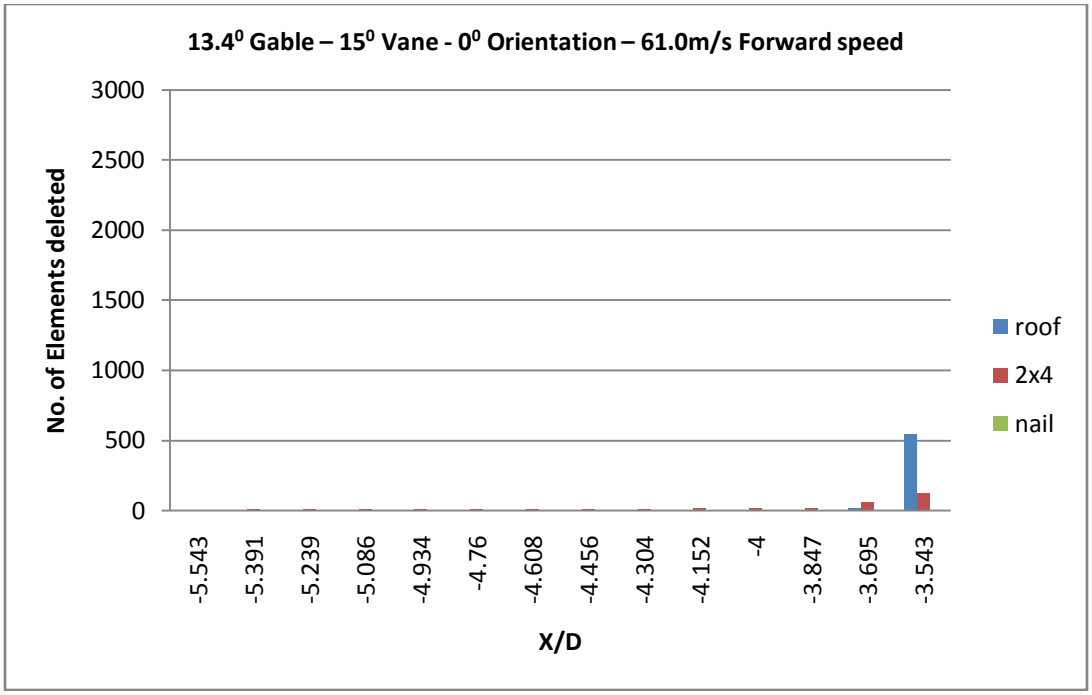

Figure 37. Number of elements failed vs. X/D for case 34

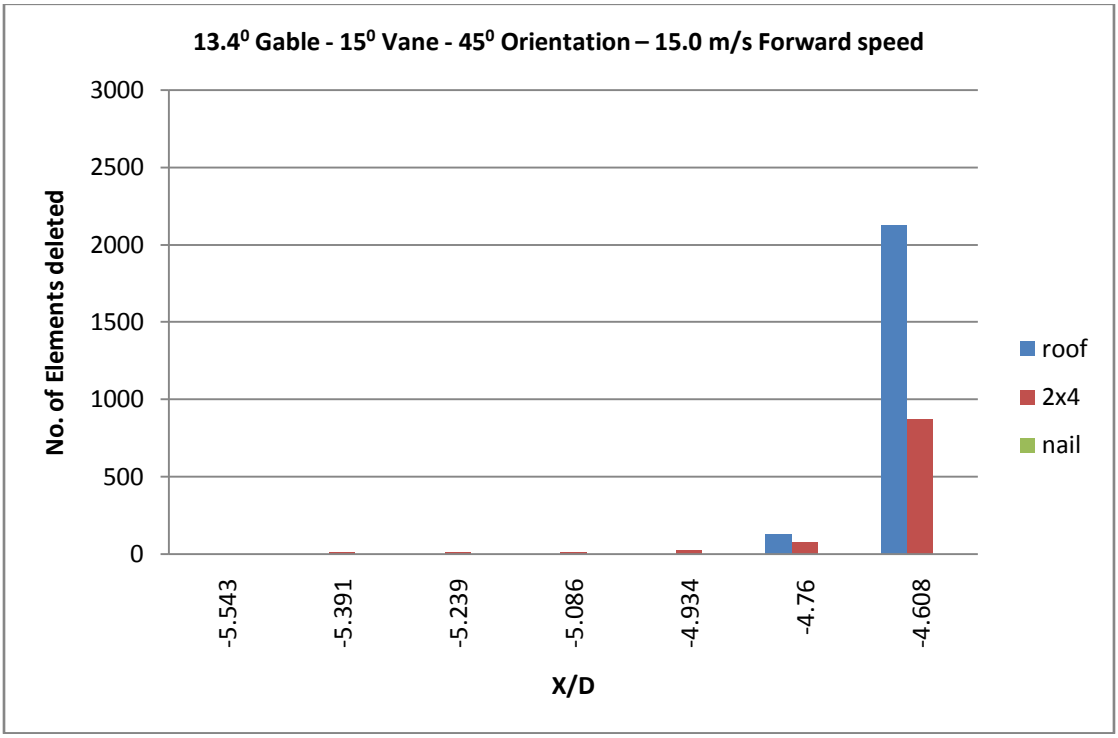

Figure 38. Number of elements failed vs. X/D for case 32

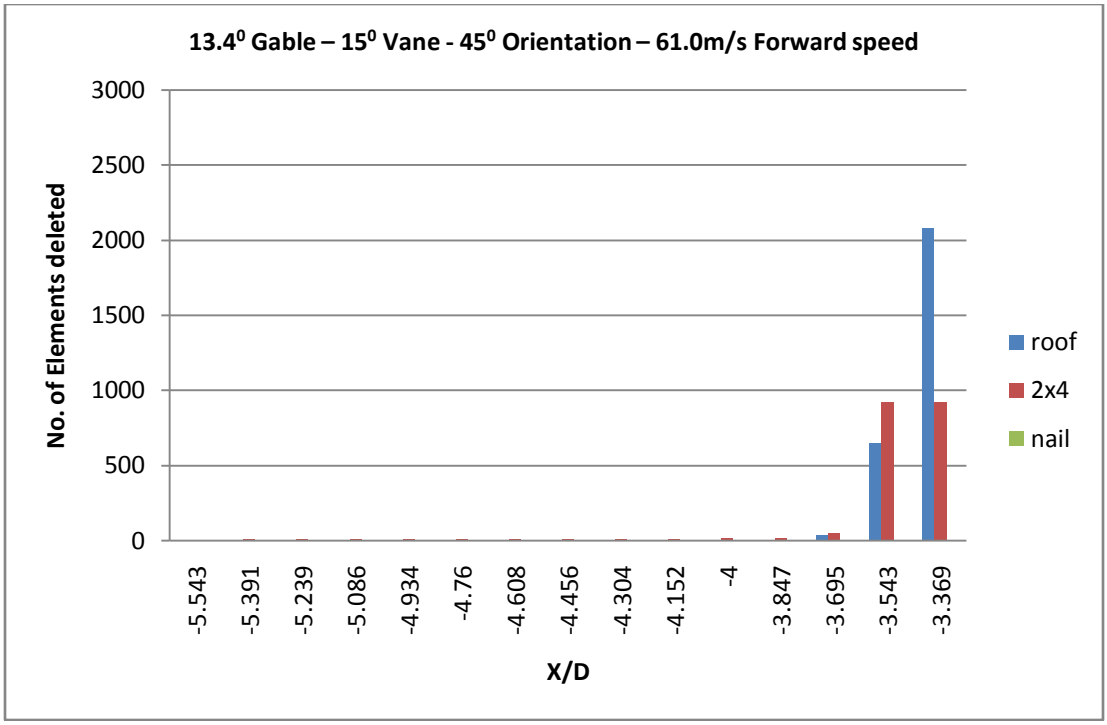

Figure 39. Number of elements failed vs. X/D for case 35

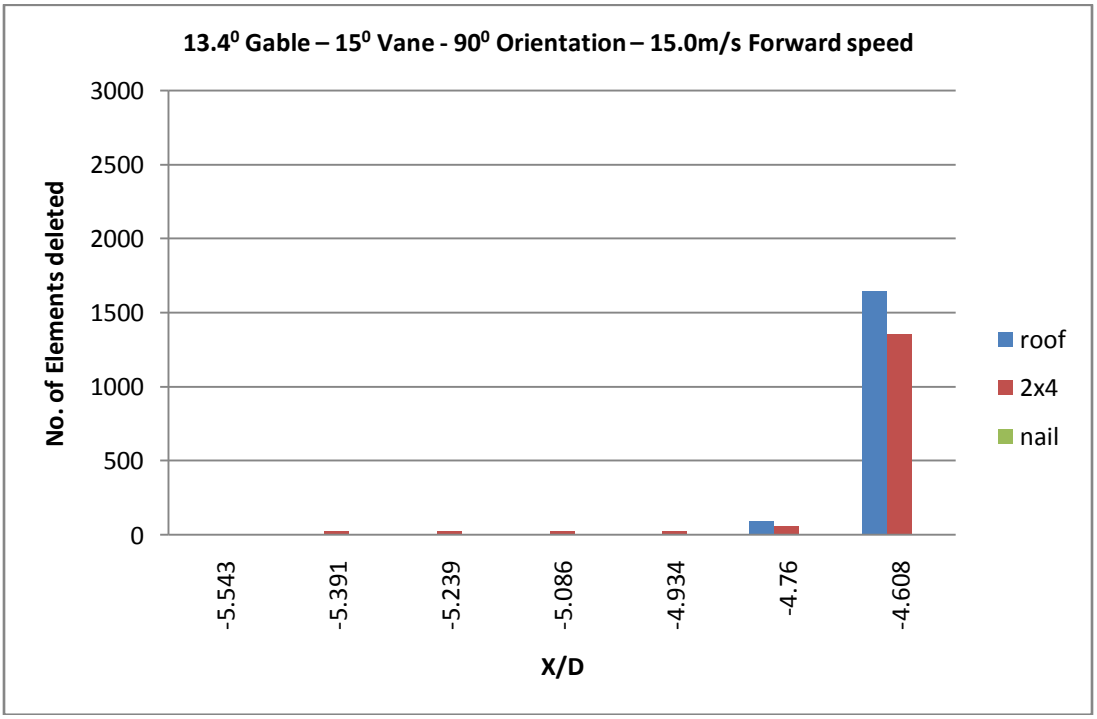

Figure 40. Number of elements failed vs. X/D for case 33

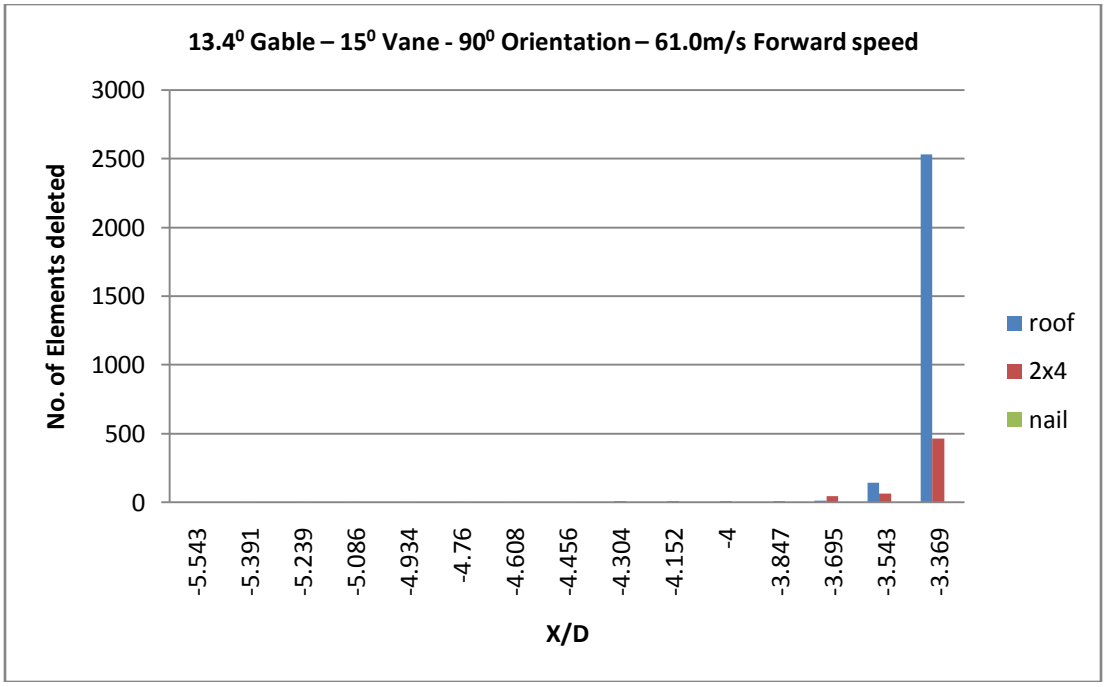

Figure 41. Number of elements failed vs. X/D for case 36

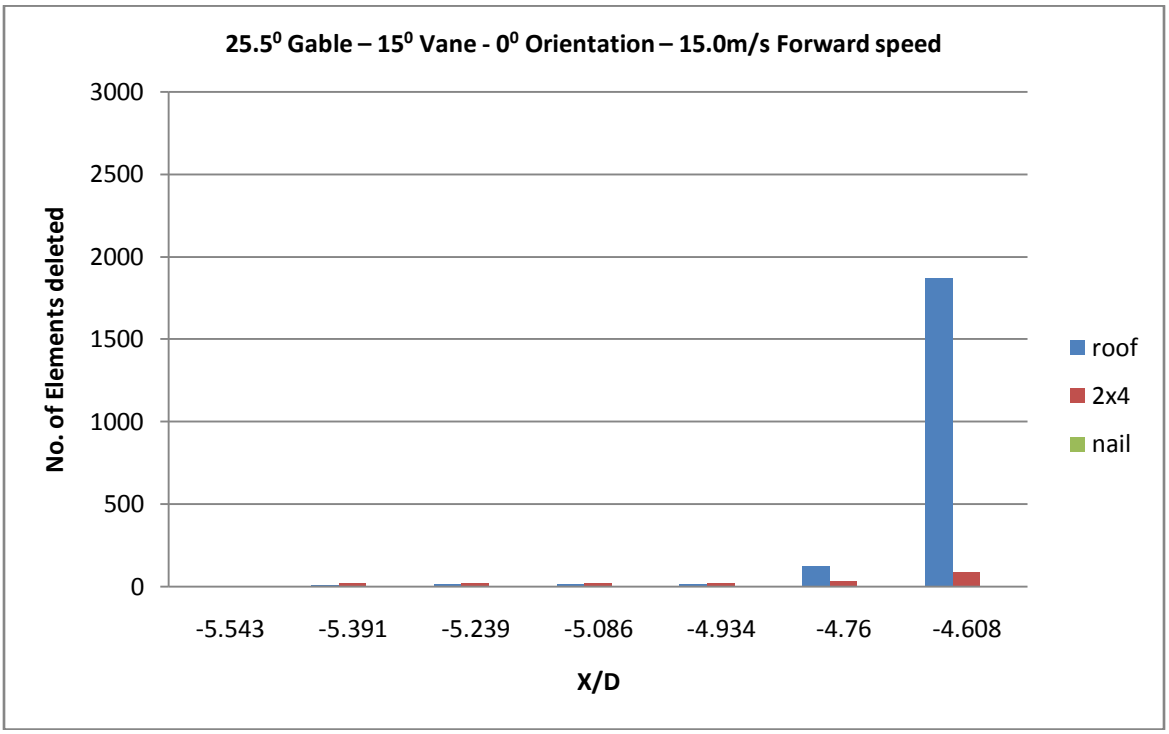

Figure 42. Number of elements failed vs. X/D for case 37

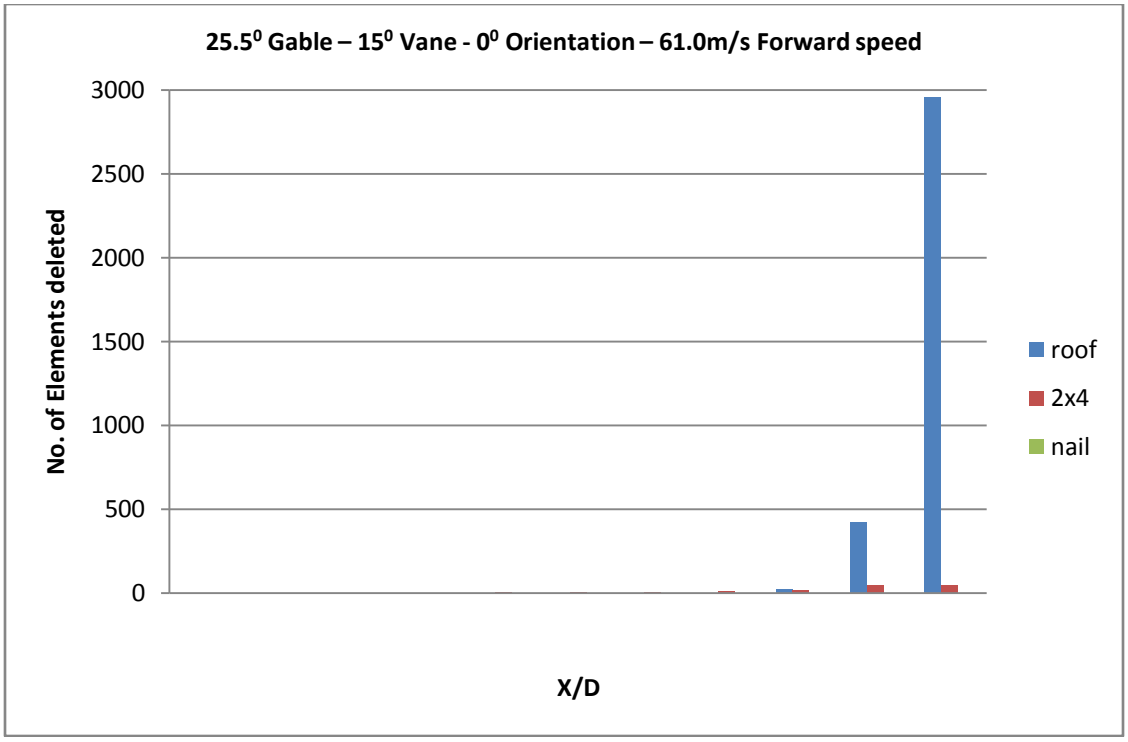

Figure 43. Number of elements failed vs. X/D for case 40

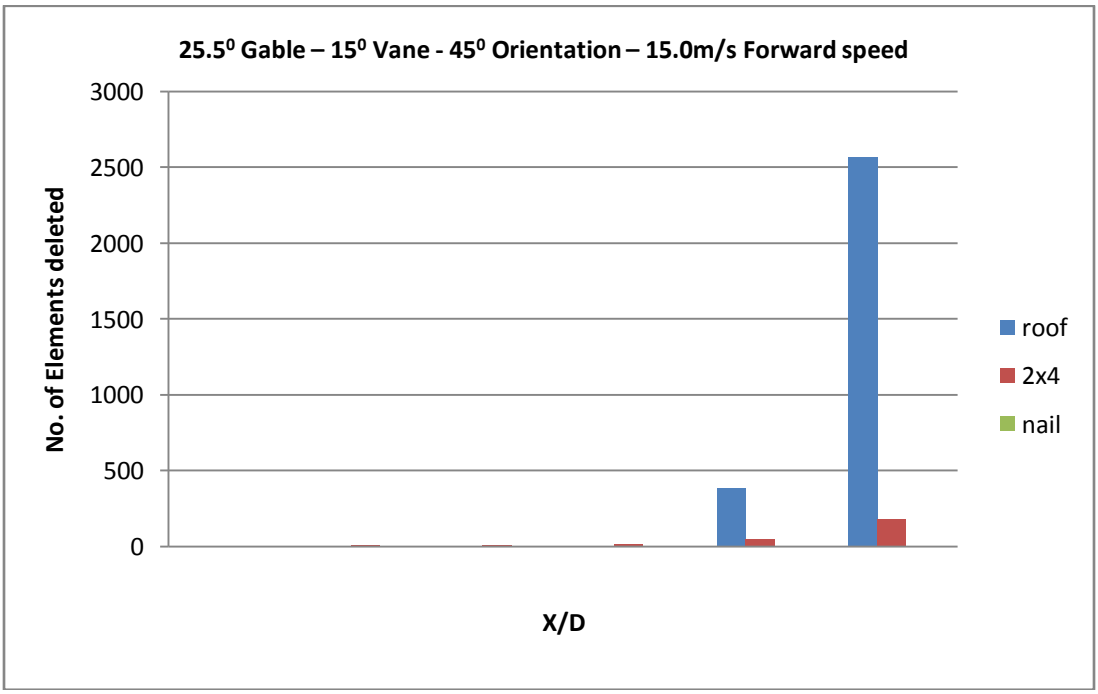

Figure 44. Number of elements failed vs. X/D for case 38

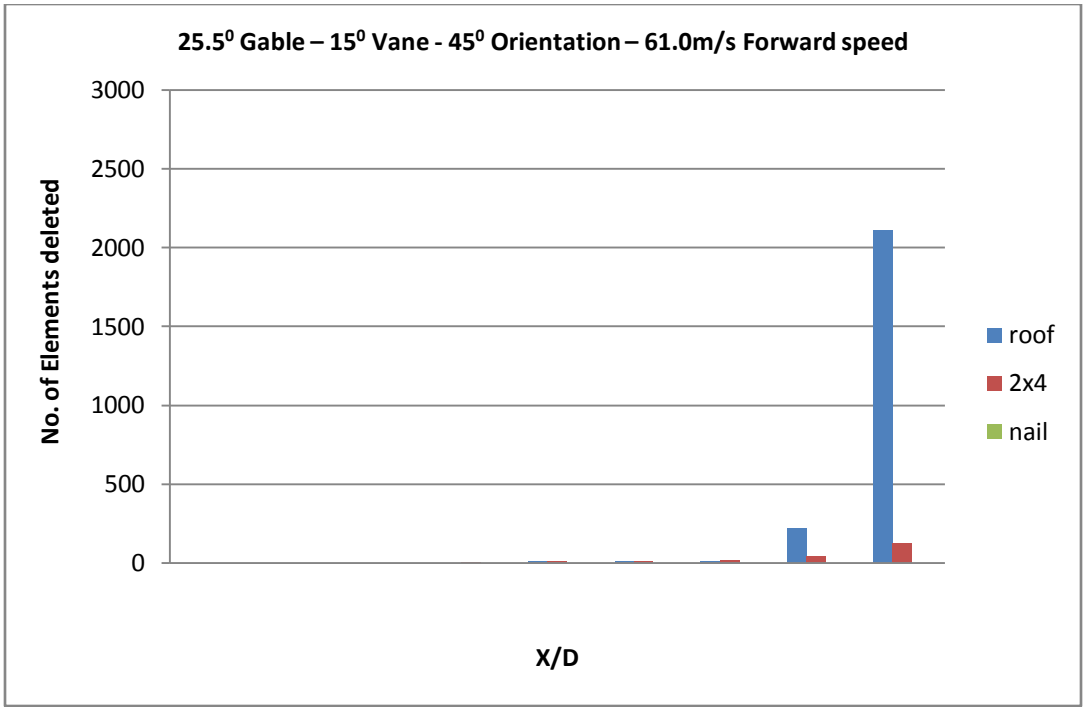

Figure 45. Number of elements failed vs. X/D for case 41

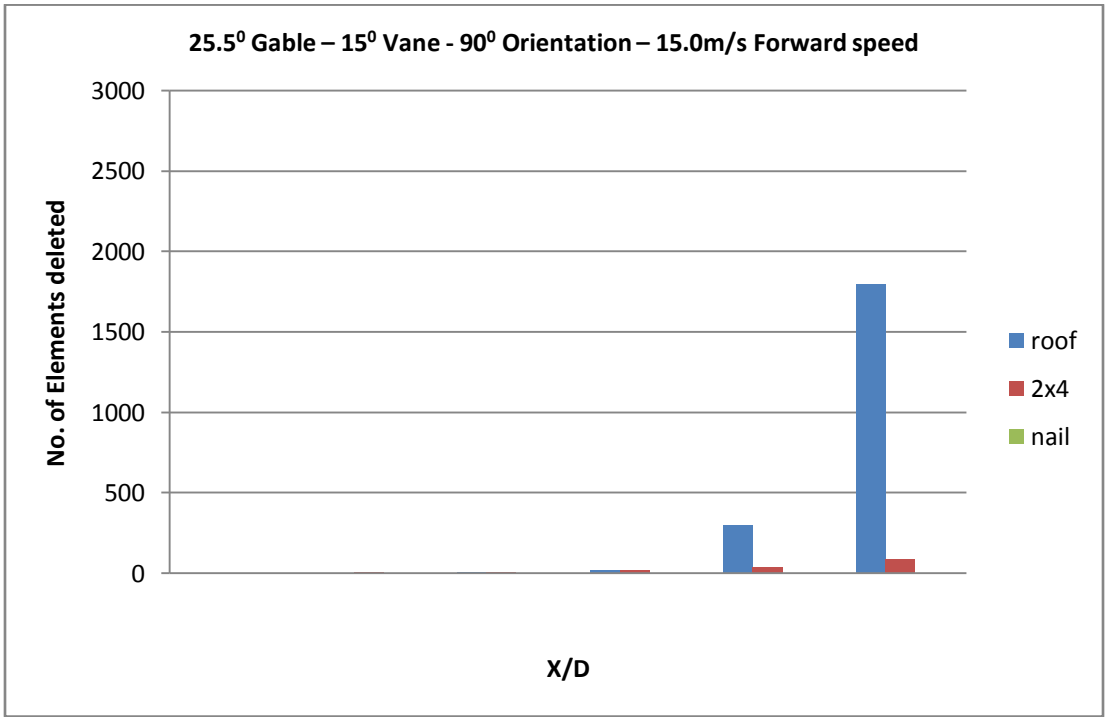

Figure 46. Number of elements failed vs. X/D for case 39

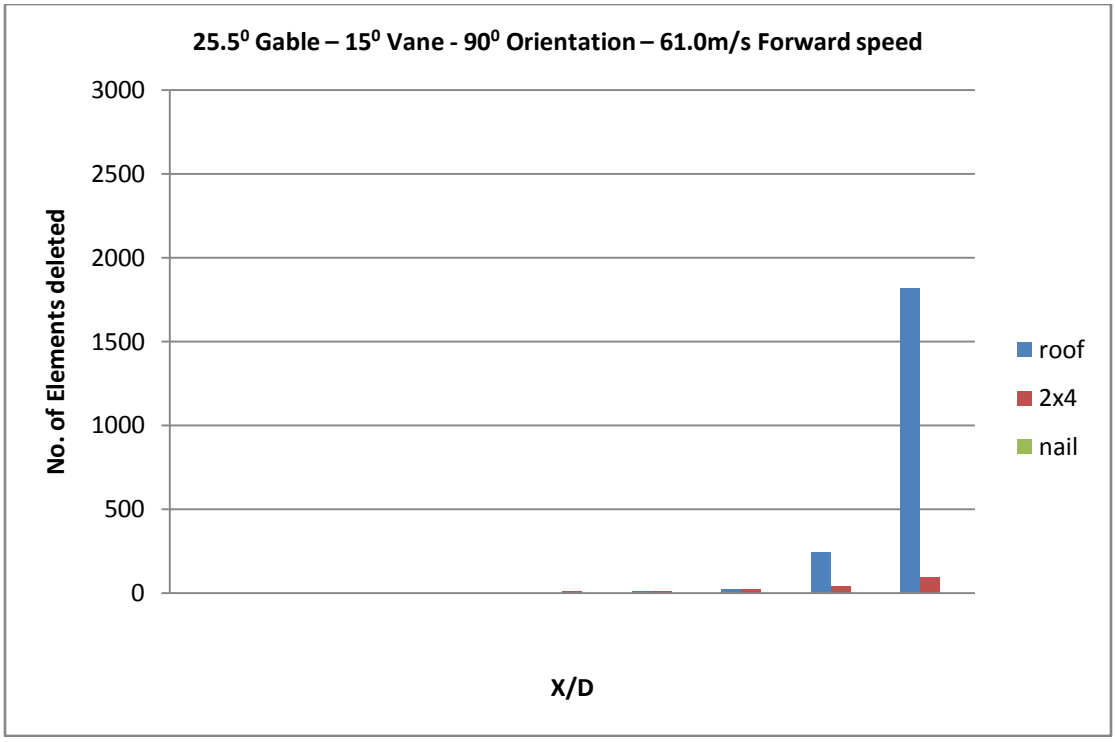

Figure 47. Number of elements failed vs. X/D for case 42

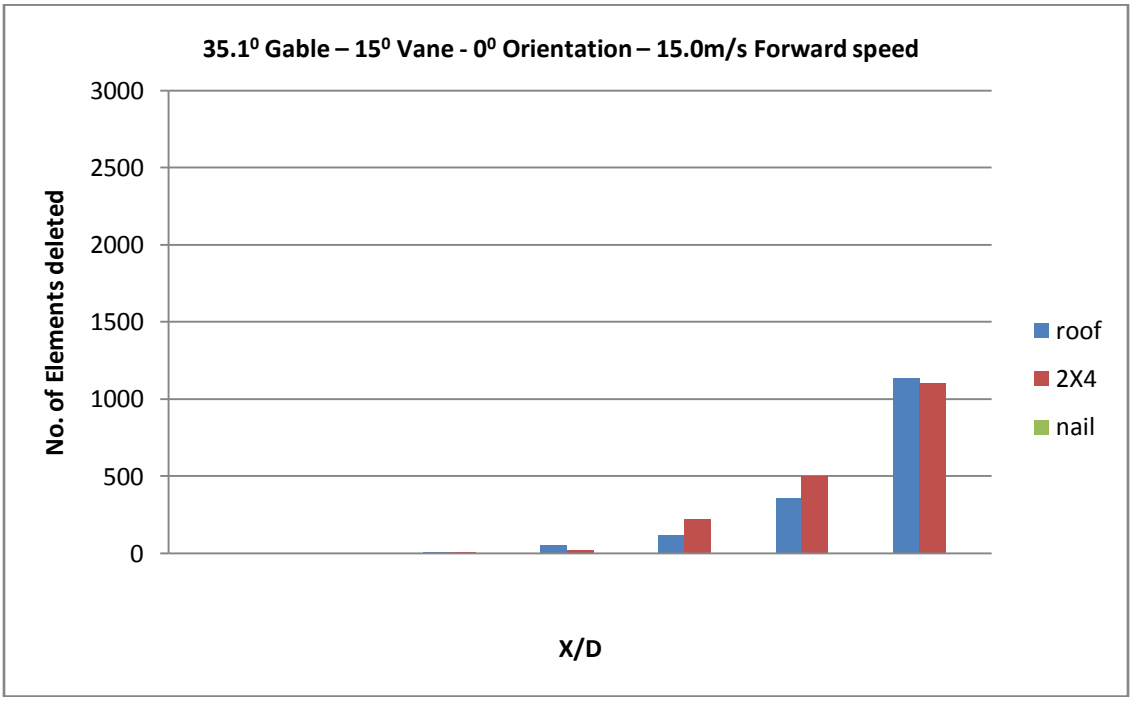

Figure 48. Number of elements failed vs. X/D for case 43

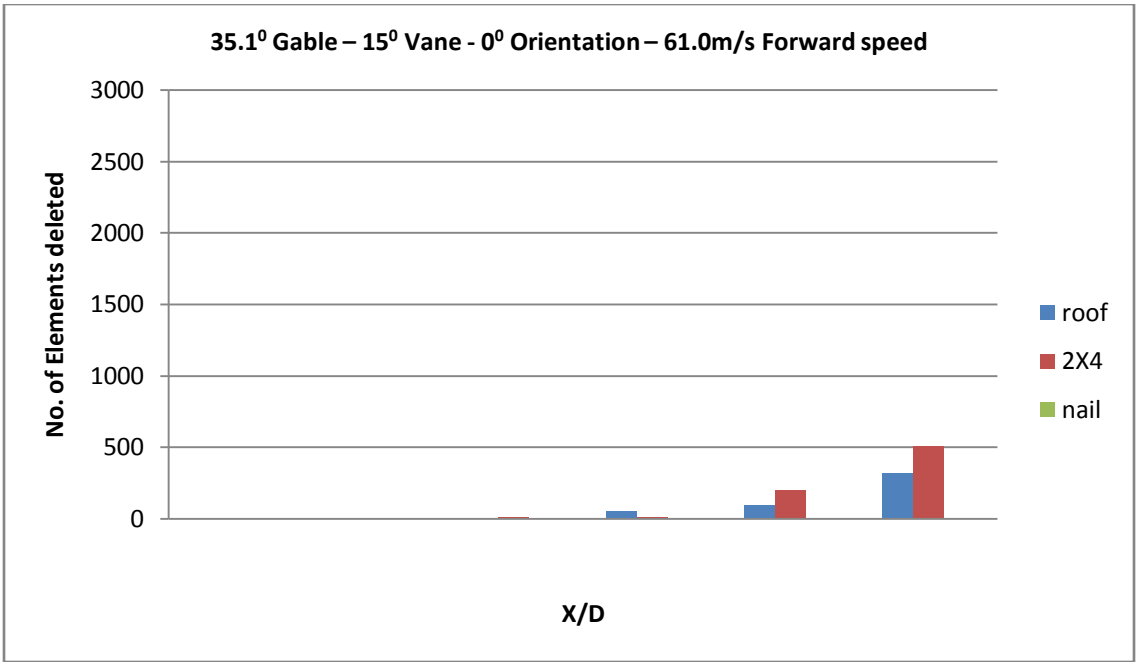

Figure 49. Number of elements failed vs. X/D for case 46

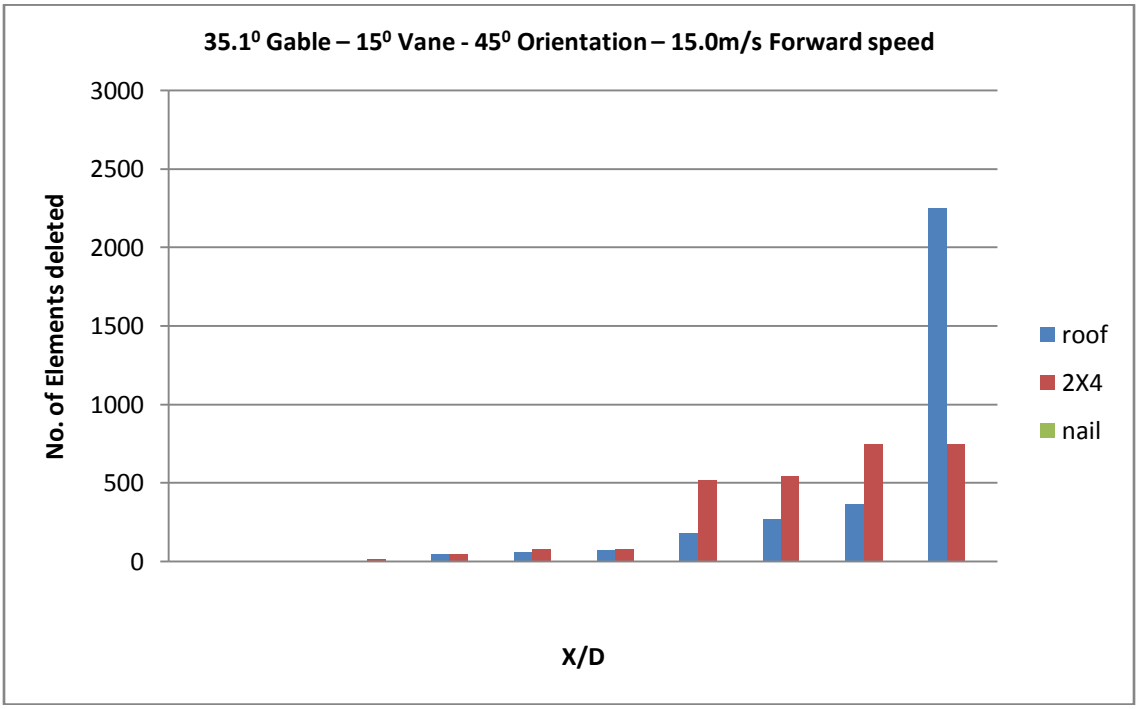

Figure 50. Number of elements failed vs. X/D for case 44

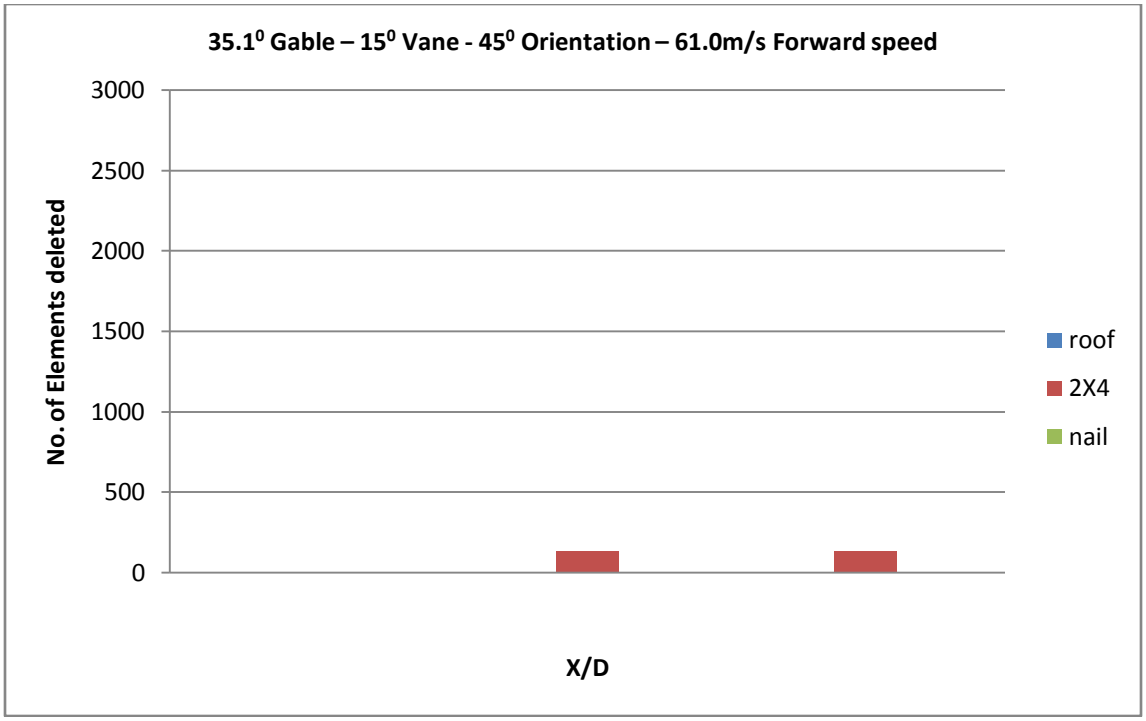

Figure 51. Number of elements failed vs. X/D for case 47

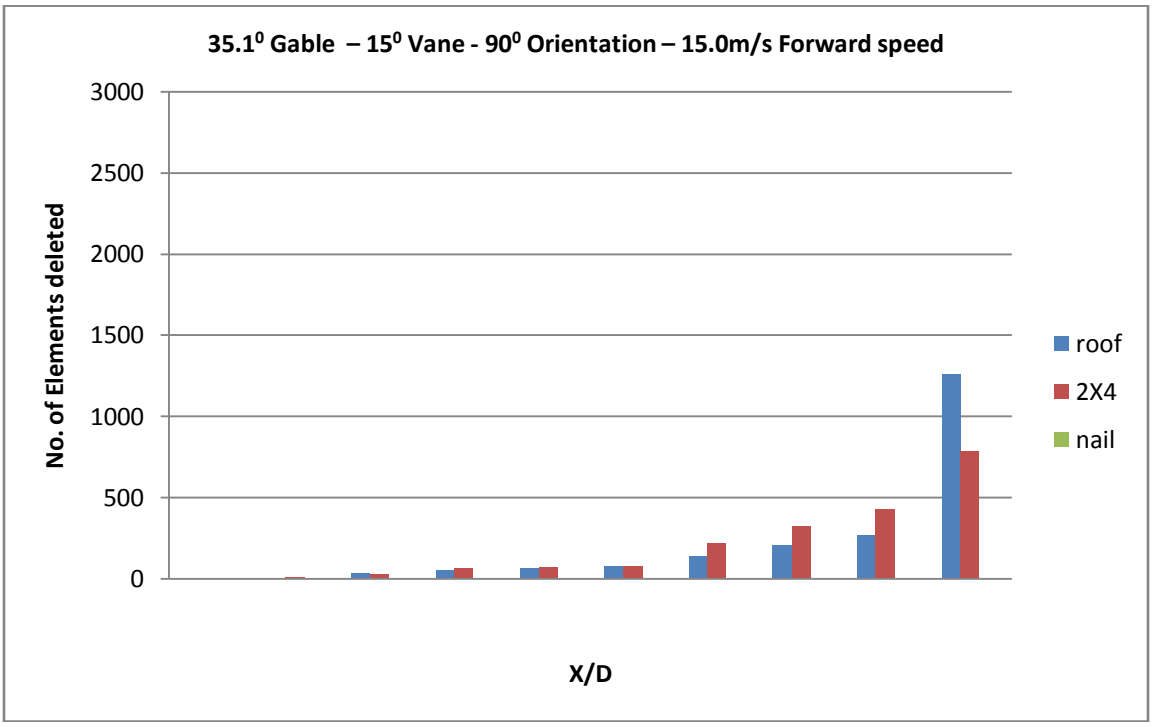

Figure 52. Number of elements failed vs. X/D for case 45

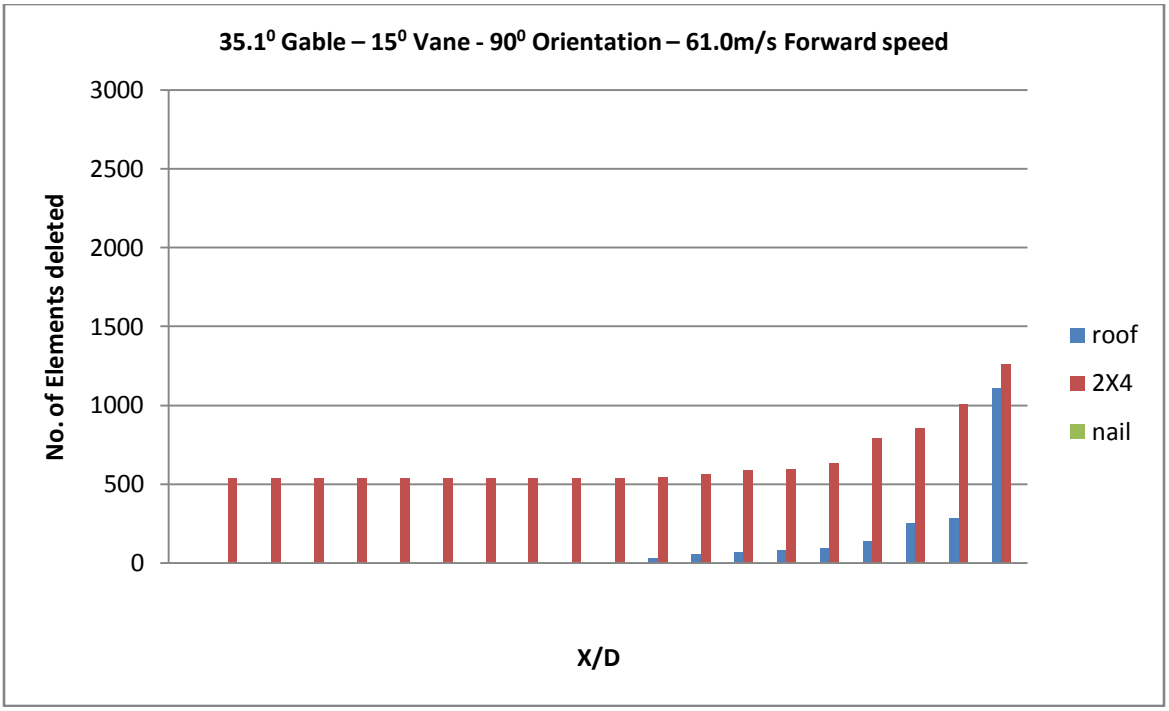

Figure 53. Number of elements failed vs. X/D for case 48

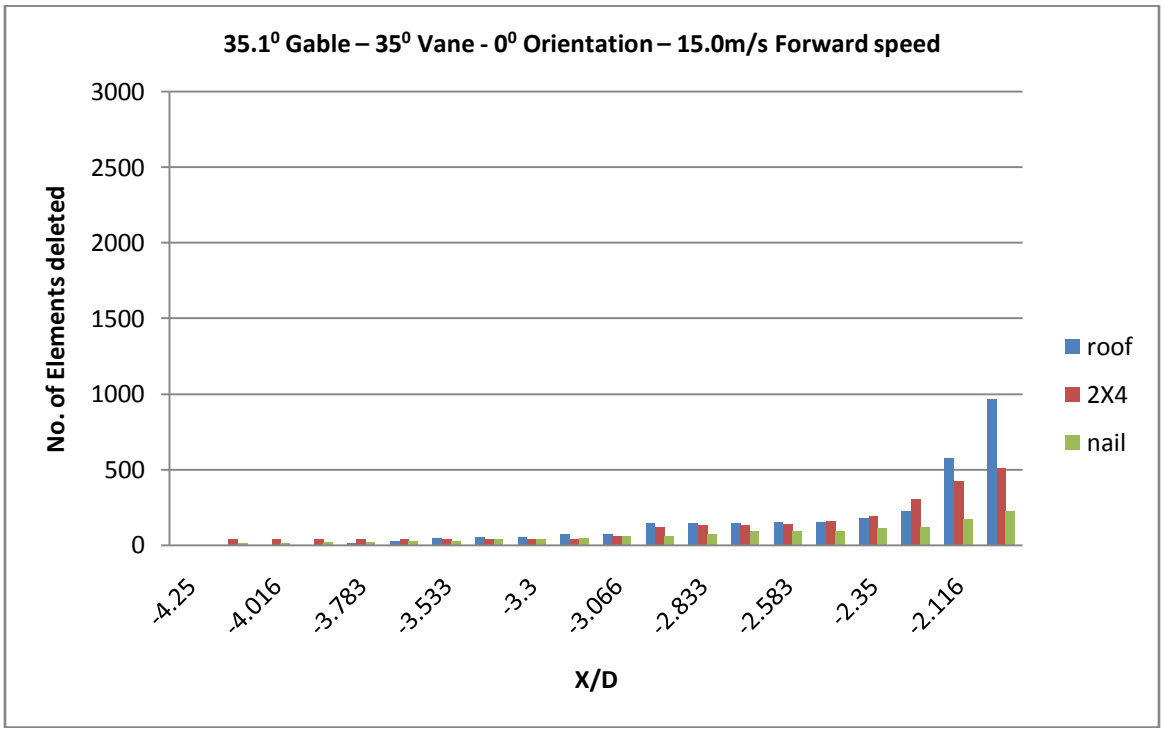

Figure 54. Number of elements failed vs. X/D for case 49

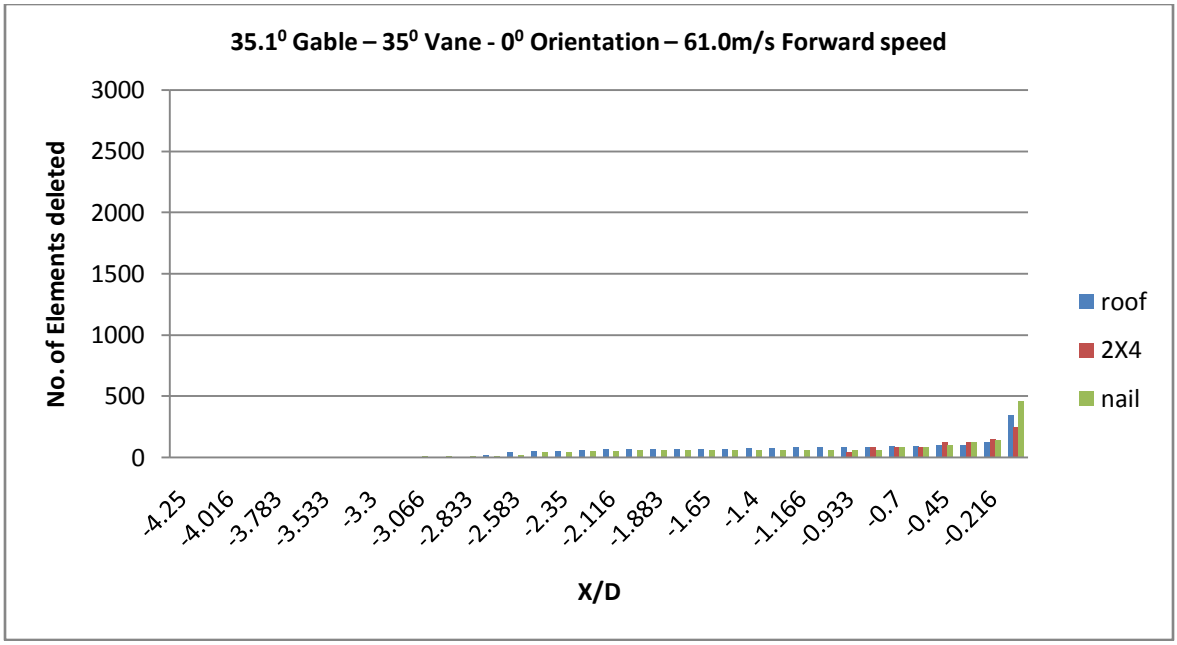

Figure 55. Number of elements failed vs. X/D for case 52

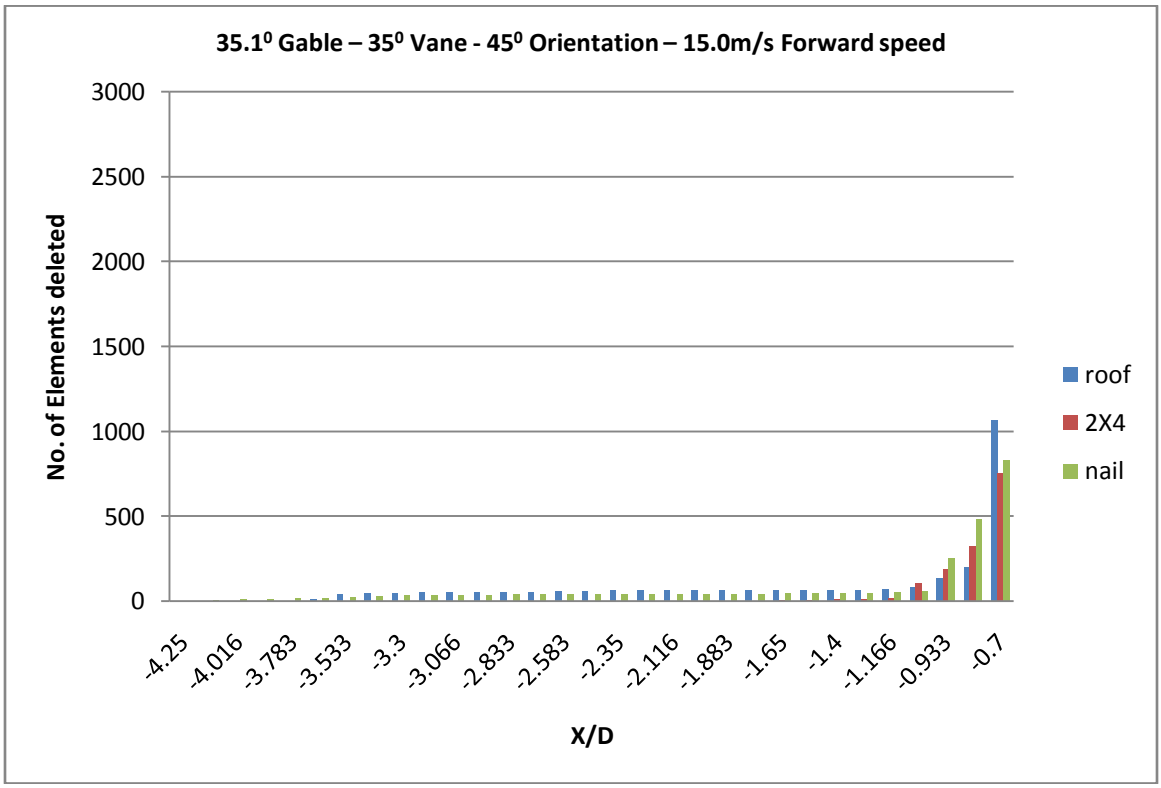

Figure 56. Number of elements failed vs. X/D for case 50

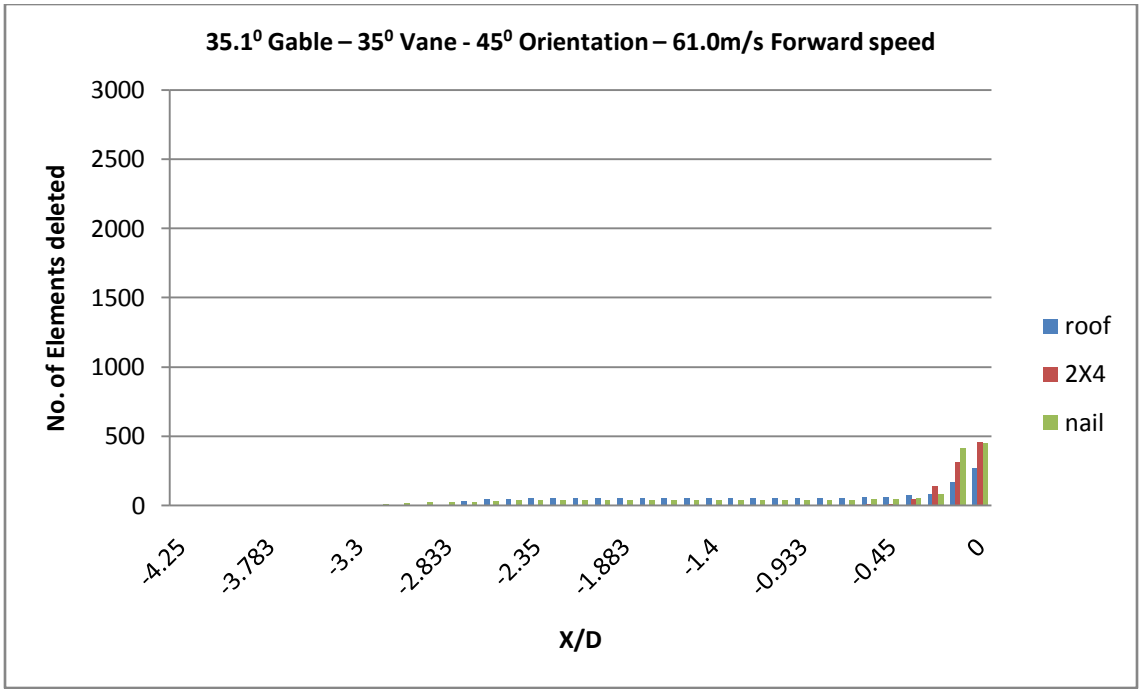

Figure 57. Number of elements failed vs. X/D for case 53

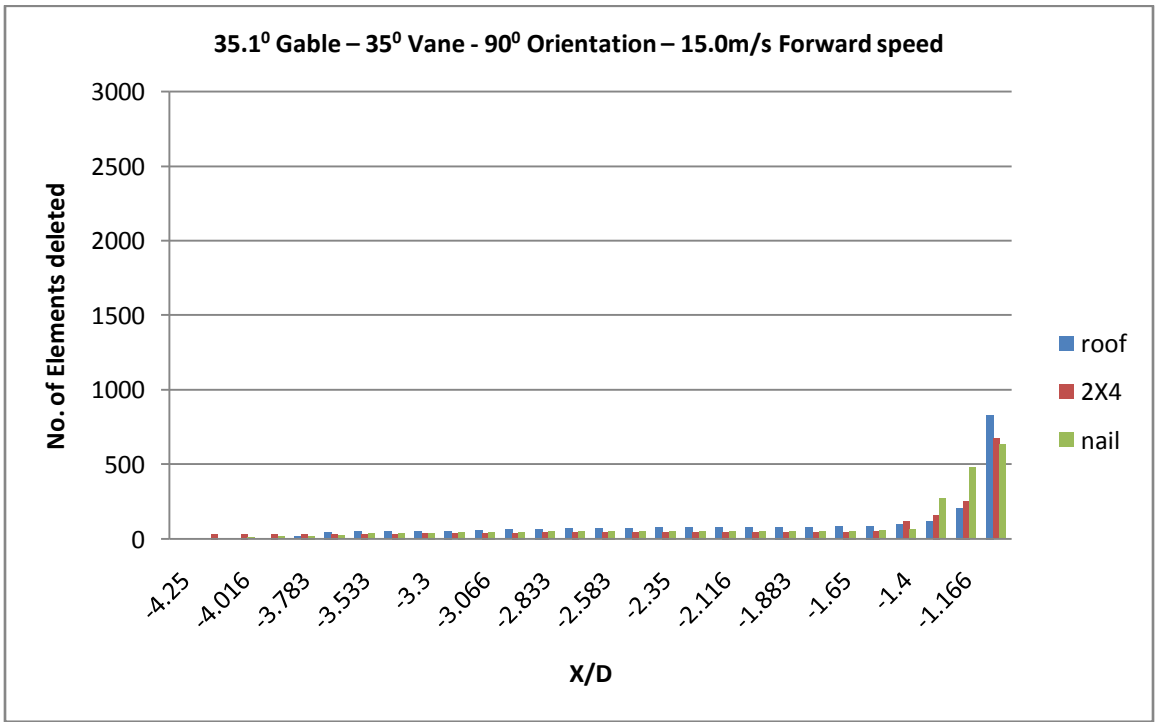

Figure 58. Number of elements failed vs. X/D for case 51

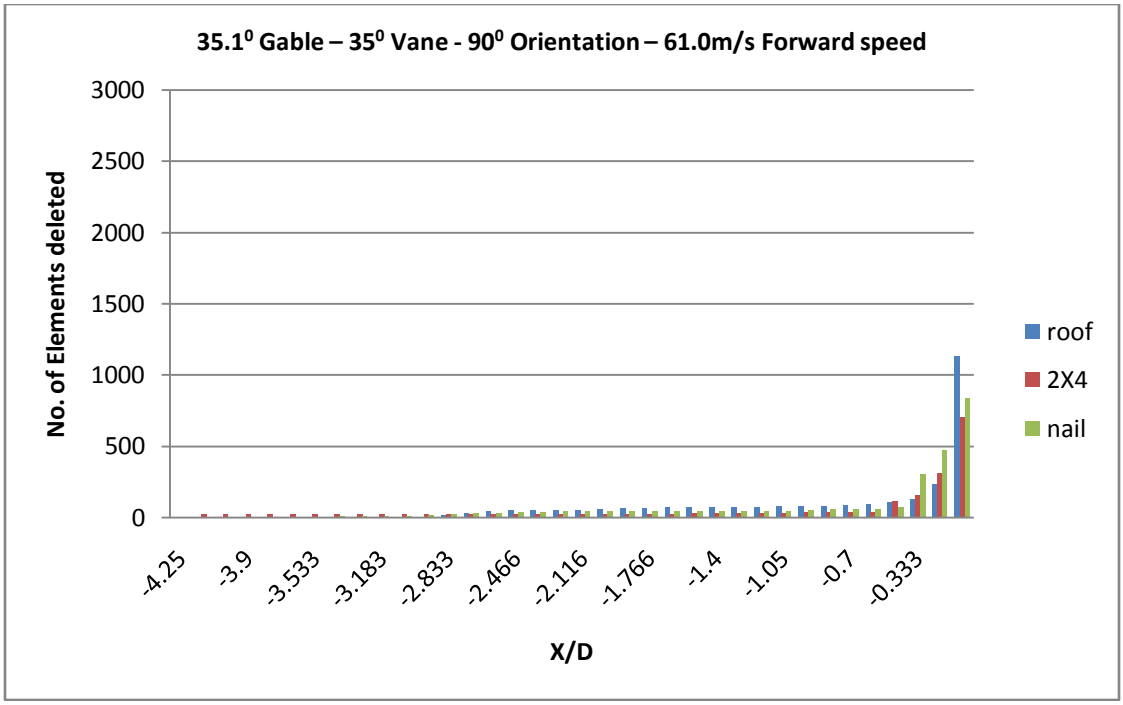

Figure 59. Number of elements failed vs. X/D for case 54

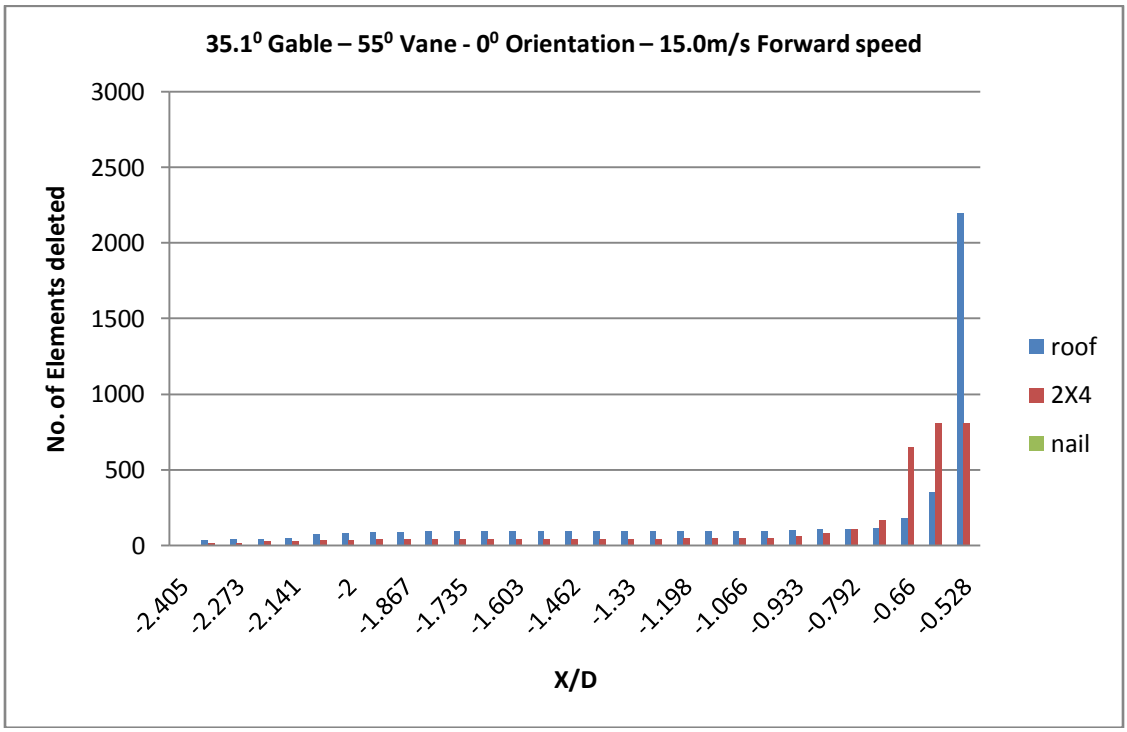

Figure 60. Number of elements failed vs. X/D for case 55

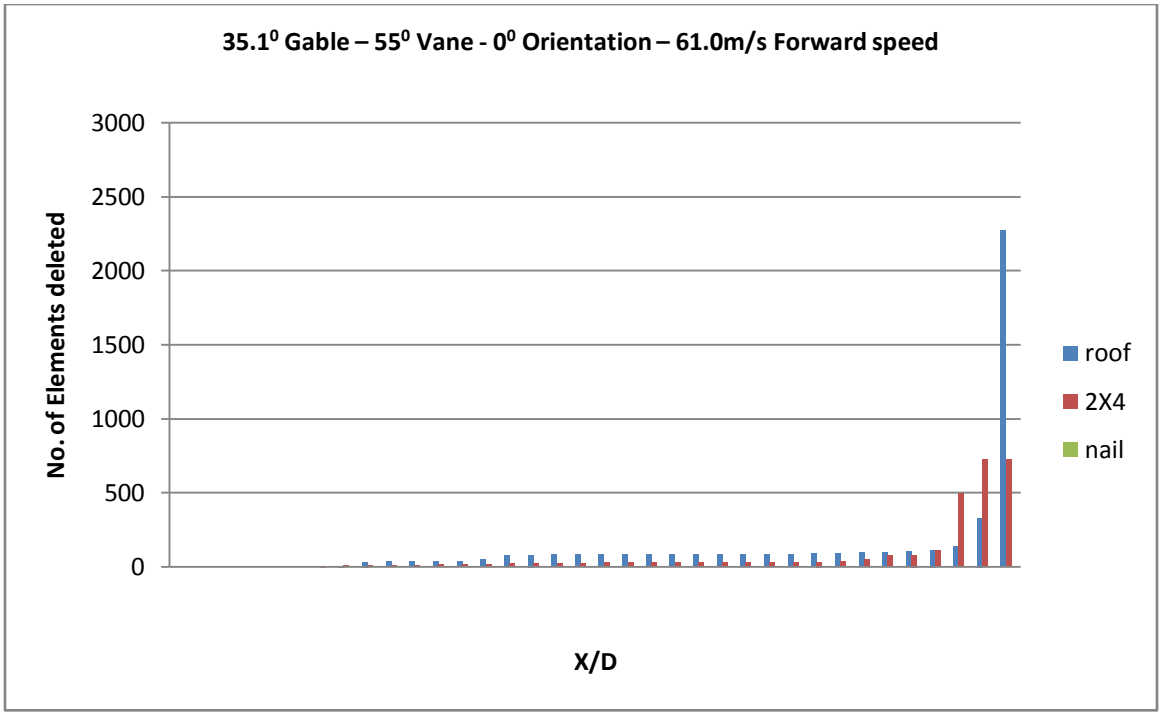

Figure 61. Number of elements failed vs. X/D for case 58

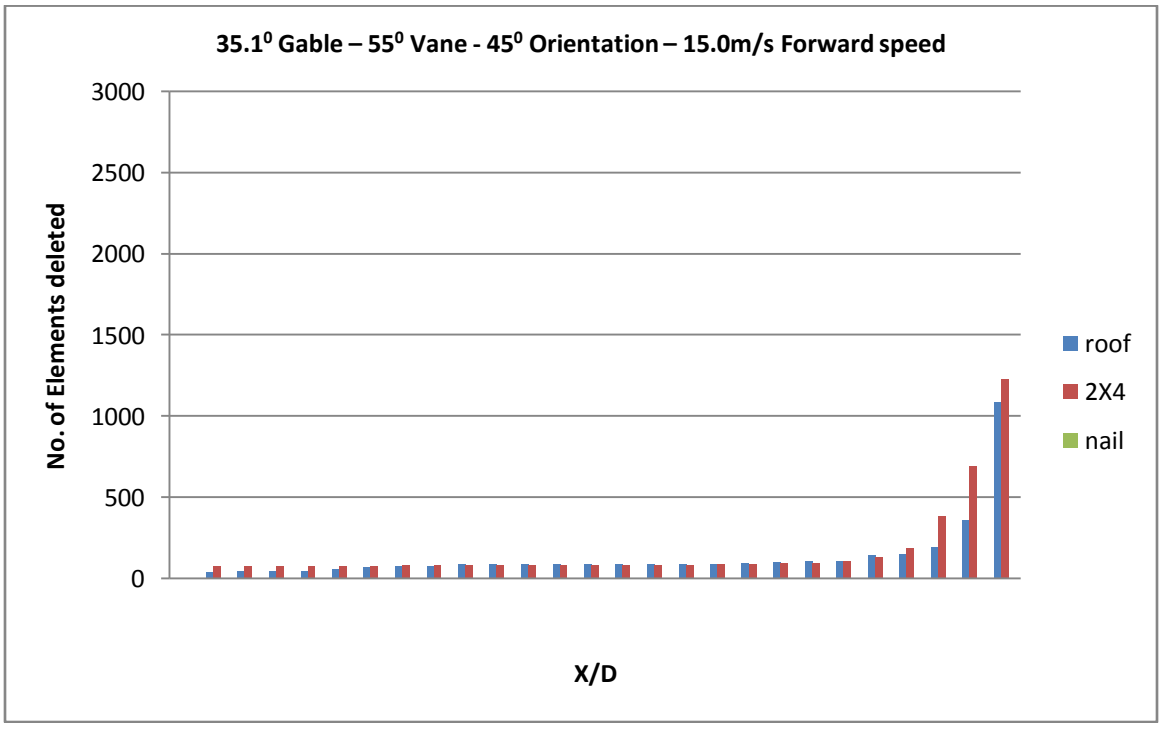

Figure 62. Number of elements failed vs. X/D for case 56

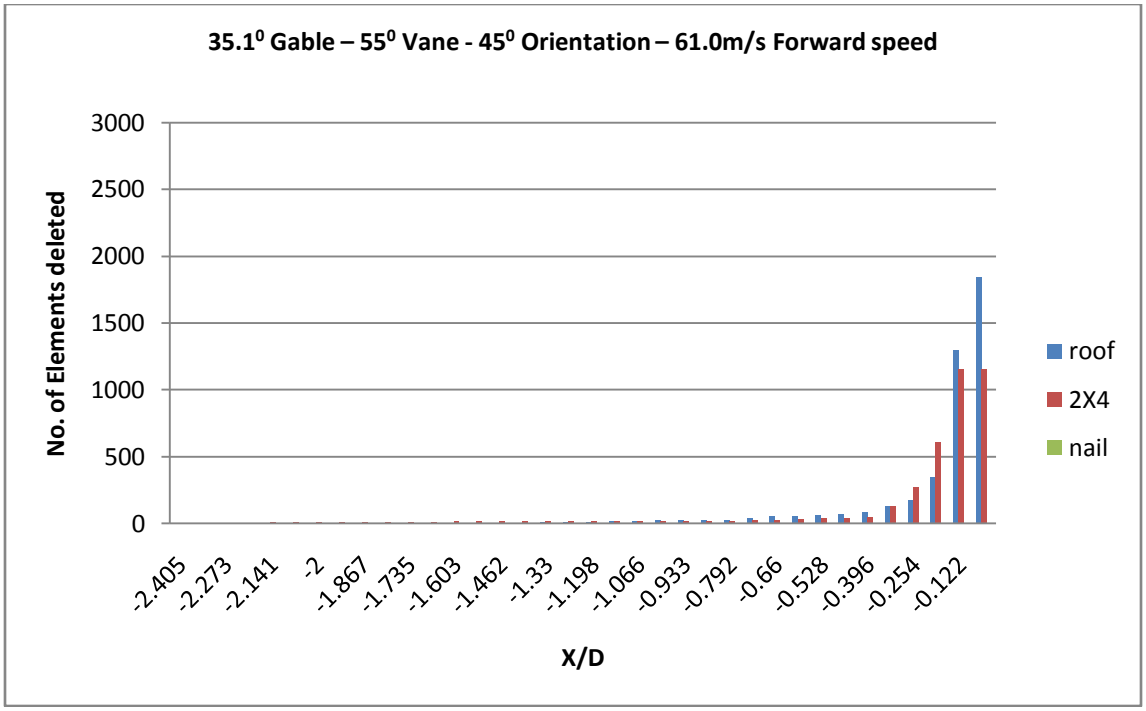

Figure 63. Number of elements failed vs. X/D for case 59

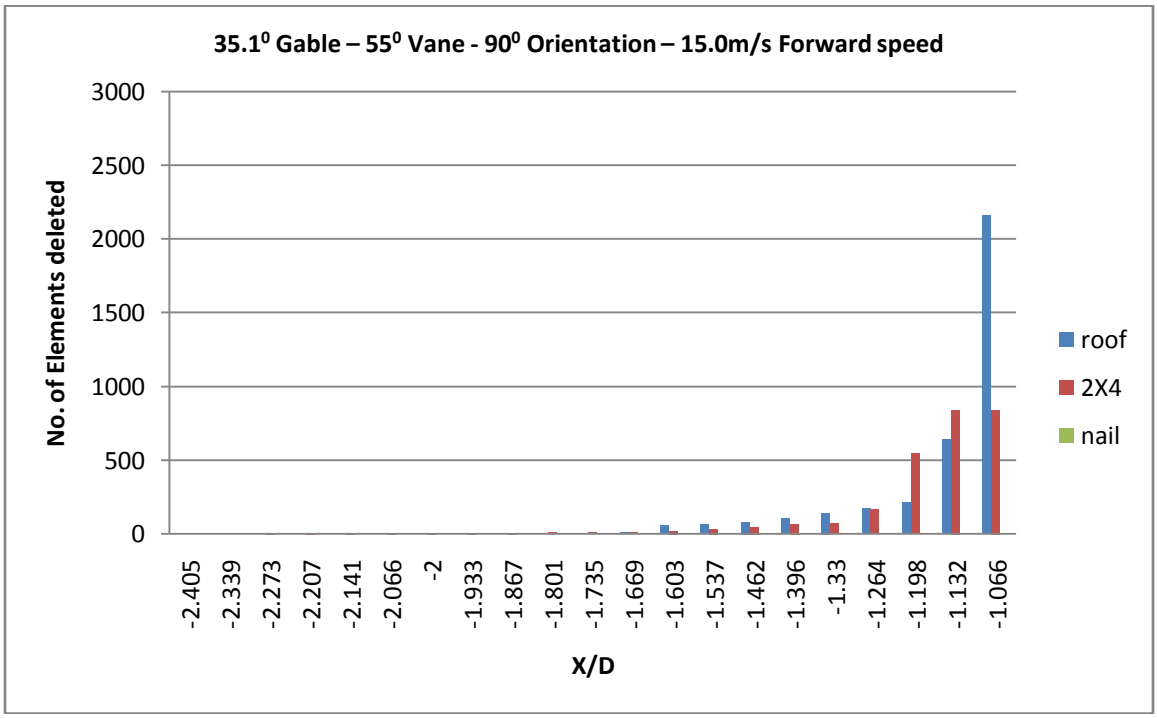

Figure 64. Number of elements failed vs. X/D for case 57

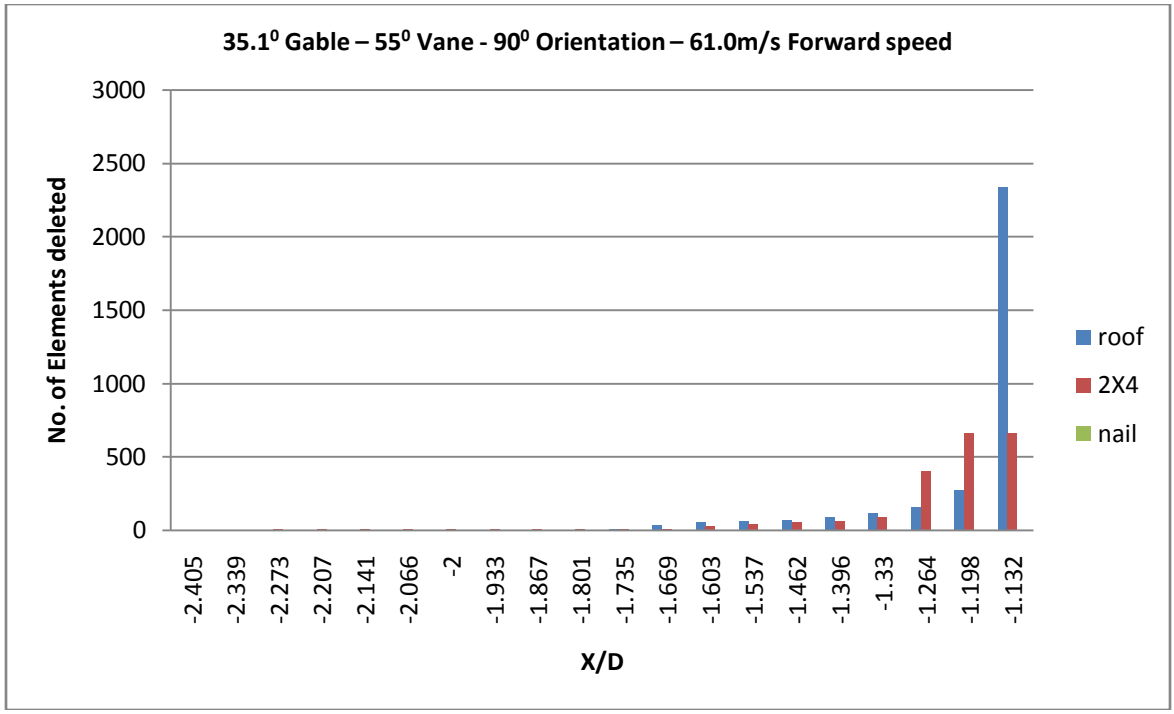

Figure 65. Number of elements failed vs. X/D for case 60

APPENDIX. SOLVER THEORY

The analysis was carried out using ANSYS 11.0. ANSYS uses the sparse solver for most structural and thermal analysis. The system of simultaneous linear equations generated by the finite element procedure is solved either using a direct elimination process or an iterative method. The sparse direct solver is the default solver for all analyses, with a few exceptions like when using electrostatic analyses for example. A direct elimination process is primarily a Gaussian elimination approach which involves solving for the unknown vector of variables {u} in (Equation 1):

$$[K]\{u\} = \{F\} \tag{1}$$

where:

[K] = global stiffness/conductivity matrix

{u} = global vector of nodal unknown

{F} = global applied load vector

The direct elimination process involves decomposition (factorization) of the matrix [K] into lower and upper triangular matrices, [K] = [L][U]. Then forward and back substitutions using [L] and [U] are made to compute the solution vector {u}.

A typical iterative method involves an initial guess, $\{u\}_1$, of the solution vector {u} and then a successive steps of iteration leading to a sequence of vectors $\{u\}_2$, $\{u\}_3$, . . . such that, in the limit, $\{u\}_n = \{u\}$ as n tends to infinity. The calculation of $\{u\}_{n+1}$ involves [K], {F}, and

the {u} vectors from one or two of the previous iterations. Typically the solution converges to within a specified tolerance after a finite number of iterations.

Direct Solvers

The two direct solvers that are available are the Sparse Direct Solver, and the Frontal (Wave front) Solver. The Sparse Direct Solver makes use of the fact that the finite element matrices are normally sparsely populated. This sparseness allows the system of simultaneous equations to be solved efficiently by minimizing the operation counts. The Frontal Solver, on the other hand, is designed to minimize the memory used in the solution process although the operation count is generally more than that of the Sparse Direct Solver. The sparse direct solver is the default solver for all analyses, with a few exceptions like when using electrostatic analyses for example.

Sparse Direct Solver

As described in the introductory section, the linear matrix equation, (Equation 1) is solved by triangular decomposition of matrix [K] to yield the following equation:

$$[L][U]\{u\} = \{F\} \qquad (2)$$

where:

[L] = lower triangular matrix

[U] = upper triangular matrix

By substituting:

$$\{w\} = [U]\{u\} \tag{3}$$

We can obtain {u} by first solving the triangular matrix system for {w} by using the forward pass operation given by:

$$[L]\{w\} = \{F\} \tag{4}$$

and then computing {u} using the back substitution operation on a triangular matrix given by:

$$[U]\{u\} = \{w\} \tag{5}$$

When [K] is symmetric, the above procedure could use the substitution:

$$[K] = [L][L]^T \tag{6}$$

However, it is modified as:

$$[K] = [L'][D][L']^T \tag{7}$$

where:

[D] = a diagonal matrix

The diagonal terms of [D] may be negative in the case of some nonlinear finite element analysis. This allows the generation of [L'] without the consideration of a square root of negative number. Therefore, (Equation 2) through (Equation 5) become:

$$[L'][D][L']^T \{u\} = \{F\} \quad (8)$$

$$\{w\} = [D][L']^T \{u\} \quad (9)$$

$$[L']\{w\} = \{F\} \quad (10)$$

and

$$[D][L']^T \{u\} = \{F\} \quad (11)$$

Since [K] is normally sparsely populated with coefficients dominantly located around the main diagonal, the Sparse Direct Solver is designed to handle only the nonzero entries in [K]. In general, during the Cholesky decomposition of [K] shown in (Equation 2) or (Equation 8), nonzero coefficients appear in [L] or [L'] at coefficient locations where [K] matrix had zero entries. The Sparse Direct Solver algorithm minimizes this fill-in by judiciously reordering the equation numbers in [K].

The performance of a direct solution method is greatly optimized through the equations reordering procedure which involves relabeling of the variables in the vector {u}. This simply amounts to permuting the rows and columns of [K] and the rows of {F} with the objective of minimizing fill-in. So, when the decomposition step in (Equation 2) or (Equation

8) is performed on the reordered [K] matrix, the fill-in that occurs in [L] or [L'] matrix is kept to a minimum. This enormously contributes to optimizing the performance of the Sparse Direct Solver.

To achieve minimum fill-in, different matrix coefficient reordering algorithms are available in the literature (George and Liu). The Sparse Direct Solver uses two different reordering schemes. They are the Minimum Degree ordering and the METIS ordering. The choice of which reordering method to use is automated in the solver algorithm in order to yield the least fill-in.

BIBLIOGRAPHY

Balaramudu V., Tornado-Induced Wind Loads On A Low-Rise Building, Master's Thesis, Department Of Aerospace Engineering, Iowa State University, December 2007.

Herzog, B., Yeh, B., Nail Withdrawal And Pull-Through Strength Of Structural –Use Panels, A.P.A – The Engineered Wood Association.

Kasal, B., Leichti, R.J., Itani, R.Y., Nonlinear Finite-Element Model Of Complete Light-Frame Wood Structures, Journal of Structural Engineering, Vol. 120, No. 1, Paper No. 5082, January 1994.

Collins, M., Kasal, B., Paevere, P., Foliente, G.C., Three-Dimensional Model Of Light Frame Wood Buildings. I: Model Description, Journal Of Structural Engineering, Pages 676 - 683, April 2005.

Collins, M., Kasal, B., Paevere, P., Foliente, G.C., Three-Dimensional Model Of Light Frame Wood Buildings. II: Model Description, Journal Of Structural Engineering, Pages 684 - 692, April 2005.

Foschi R.O., Analysis Of Wood Diaphragms And Trusses, Part I: Diaphragms, Canadian Journal of Civil Engineering, Vol. 4, No. 3, Pages 345 - 352.

Foliente, G.C., Hysterisis Modeling Of Wood Joint And Structural Systems, Journal of Structural Engineering, Vol. 121, No. 6, June 1995.

Gupta, A. K., and Kuo, G. P., Modeling Of A Wood-Framed House, Journal Of Structural Engineering, 113(2), Pages 260 – 278, 1987.

He, M., Lam, F., and Foschi, R.O., Modeling Three-Dimensional Timber Light-Frame Buildings, Journal Of Structural Engineering., 127(8), Pages 901 – 913, 2001.

Kasal B., A Nonlinear Three-Dimensional Finite-Element Model Of A Light-Frame Wood Structure, Ph.D. thesis, Oregon State University, Corvallis, Oregon, USA, 1992.

MatWeb, Material Property Data, http://www.matweb.com.

He, M., Lam, F., Foschi, R.O., Modeling Three-Dimensional Timber Light-Frame Buildings, Journal Of Structural Engineering, Pages 901 - 913, August 2001.

Aune, P., Patton-Mallory, M., Lateral Load-Bearing Capacity Of Nailed Joints Based On The Yield Theory - Experimental Verification, United States Department of Agriculture, Research Paper FPL 470.

Paevere, P.J., Foliente, G.C, Kasal, B., Load-Sharing And Redistribution In A One-Story Wood-Frame Building, Journal Of Structural Engineering, ASCE, Pages 1275 - 1284, September 2003.

Plywood Design Specification, APA – The Engineered Wood Association.

Chow, P., McNatt, J.D., Lambrechts, S. J., Gertner, G. Z., Direct Withdrawal And Head Pull-Through Performance Of Nails And Staples In Structural Wood-Based Panel Materials, Forest Products Journal, Vol. 38, No. 6.

ANSYS Inc, ANSYS Release 11.0 Documentation.

Sarkar P., Reducing wind induced damages from storms, NOAA proposal.

Tuomi, R. L., and McCutcheon, W. J. Testing of full-scale house under simulated snow loads and wind loads. Research Paper FPL 234, Forest Products Laboratory, USDA Forest Service, Madison, Wisconsin, 1974.

ACKNOWLEDGEMENTS

I would like to take this opportunity to express my thanks to those who helped me with various aspects of conducting research and the writing of this thesis. First and foremost, Dr. Vinay Dayal for his guidance, patience and support throughout this research and the writing of this thesis. His insights and words of encouragement have often inspired me and renewed my hopes for completing my graduate education. I would like to thank my committee members for their efforts and contributions to this work: Dr. Partha Sarkar and Dr. William Gallus. I would also like to thank Dr. Fred Haan and Vasanth Balaramudu whose experimental work is the basis of this thesis. On a personal note, thanks to my friends at Iowa State and most importantly my parents and my brother for their love, help and support.